Inorganic Chemistry
Article

Inorg. Chem. **2011**, *50*, 285–298 **285**
DOI: 10.1021/ic101934t

Synthesis, Dynamic Behavior, and Reactivity of New Unsaturated Heterotrinuclear 46 Valence Electron Complexes†

Juan Forniés,* Consuelo Fortuño,* Susana Ibáñez, Antonio Martín, and Pilar Romero

Departamento de Química Inorgánica and Instituto de Ciencia de Materiales de Aragón, Universidad de Zaragoza, CSIC, 50009 Zaragoza, Spain

Piero Mastrorilli* and Vito Gallo

Dipartimento di Ingegneria delle Acque e di Chimica del Politecnico di Bari, via Orabona 4, I-70125 Bari, Italy.

Received September 21, 2010

The reaction of $[NBu_4]_2[(C_6F_5)_2Pt(\mu\text{-}PPh_2)_2Pd(\mu\text{-}PPh_2)_2Pt(C_6F_5)_2]$ (**1a**) with $[AgPPh_3]^+$ results in the oxidation of two bridging diphenylphosphanides to give the 46e species $[(PPh_3)(C_6F_5)_2Pt^2(\mu\text{-}P^2Ph_2)Pd(\mu\text{-}PPh_2)(\mu\text{-}Ph_2P^4\text{—}P^3Ph_2)Pt^1(C_6F_5)_2]$ (**3**). Complex **3** displays two tetracoordinated terminal platinum centers and a central Pd atom that is bonded to three P atoms and that completes its coordination sphere by a rather long (3.237 Å) dative $Pt^2 \rightarrow Pd$ bond. Complex **3** is also obtained when $[(R_F)_2Pt(\mu\text{-}PPh_2)Pd(\mu\text{-}PPh_2)(\mu\text{-}Ph_2P\text{-}PPh_2)Pt(R_F)_2]$ (**2**) is reacted with PPh_3. Analogously, the addition of PPh_2Et, CO or pyridine to **2** affords the 46e complexes of general formula $[(L)(C_6F_5)_2Pt^2(\mu\text{-}P^2Ph_2)Pd(\mu\text{-}PPh_2)(\mu\text{-}Ph_2P^4\text{—}P^3Ph_2)Pt^1(C_6F_5)_2]$ (L = PPh_2Et, **4**; L = CO, **6**; L = pyridine, **7**). The geometry around Pt^2 is determined by the bulkiness of L bonded to Pt. Thus, in complexes **3** (L = PPh_3) and **4** (L = PPh_2Et), the ligand L occupies the trans position with respect to μ-P^2, and in **6** (L = CO), the ligand L occupies the cis position with respect to μ-P^2. Interestingly, for **7** (L = py), both isomers **7**-*trans* and **7**-*cis*, could be isolated. Although **4** did not react with an excess of PPh_2Et, the reaction with the less sterically demanding CH_3CN ligand resulted in the opening of the $Pt^2\text{—}P^2\text{—}Pd$ cycle with formation of the saturated 48e species $[(PPh_2Et)(C_6F_5)_2Pt(\mu\text{-}PPh_2)Pd(MeCN)(\mu\text{-}PPh_2)(\mu\text{-}Ph_2P\text{-}PPh_2)Pt(C_6F_5)_2]$ (**8**). The saturated 48e complex $[(CO)(C_6F_5)_2Pt(\mu\text{-}PPh_2)Pd(MeCN)(\mu\text{-}PPh_2)(\mu\text{-}Ph_2P\text{-}PPh_2)Pt(C_6F_5)_2]$ (**9**) was obtained by acetonitrile addition to **6**. Beside the hindered rotation of the pentafluorophenyl groups and a flip-flop motion of the $Pd\text{—}P\text{—}Pt^1\text{—}P\text{—}P$ ring observed at low *T*, a rotation about the $Pt^2\text{—}P^2$ bond and a P—C oxidative addition/reductive elimination process occur for **3** and **4** at room temperature. A "through-space" $^{19}F\text{—}^{31}P$ spin—spin coupling between an *ortho*-F and the P^4 is observed for complexes **3** and **4**, having the C_6F_5 groups bonded to Pt^2 in mutually trans position. The XRD structures of complexes **3**, **6**, **7**-*trans*, **7**-*cis*, **8**, and **9** are described.

Introduction

Anionic platinate(II) complexes react with silver compounds, such as AgXL (L = PPh_3, thf; X = ClO_4, OTf), forming polynuclear complexes endowed with Pt—Ag donor—acceptor bonds, which in some cases, evolve through electron transfer reactions resulting in the oxidation of the platinate substrates.[2−11] These processes were found to depend on the silver source used and perceptible differences have been observed passing, for instance, from $AgClO_4$ to $[AgOClO_3(PPh_3)]$.[12]

† Polynuclear Homo- or Heterometallic Palladium(II)—Platinum(II) Pentafluorophenyl Complexes Containing Bridging Diphenylphosphido Ligands. 27. For part 26, see ref 1.

*To whom correspondence should be addressed. E-mail: juan.fornies@unizar.es (J.F.); cfortuno@unizar.es (C.F.); p.mastrorilli@poliba.it (P.M.).

(1) Alonso, E.; Forniés, F.; Fortuño, C.; Lledós, A.; Martín, A.; Nova, A. *Inorg. Chem.* **2009**, *48*, 7679–7690.
(2) Forniés, J.; Martín, A. In *Metal Clusters in Chemistry*; Braunstein, P., Oro, L. A., Raithby, P. R., Eds.; Wiley-VCH: Weinheim, Germany, 1999; Vol. *1*, pp 417−443.
(3) Connelly, N. G.; Geiger, W. E. *Chem. Rev.* **1996**, *96*, 877–910.
(4) Ebihara, M.; Iiba, M.; Matsuoka, H.; Okuda, C.; Kawamura, T. *J. Organomet. Chem.* **2004**, *689*, 146–153.
(5) Liu, F. H.; Chen, W. Z.; Wang, D. Q. *Dalton Trans* **2006**, 3015–3024.
(6) Oberbeckmann-Winter, N.; Morise, X.; Braunstein, P.; Welter, R. *Inorg. Chem.* **2005**, *44*, 1391–1403.
(7) Alonso, E.; Forniés, J.; Fortuño, C.; Martín, A.; Orpen, A. G. *Organometallics* **2003**, *22*, 5011–5019.
(8) Falvello, L. R.; Forniés, J.; Fortuño, C.; Durán, F.; Martín, A. *Organometallics* **2002**, *21*, 2226–2234.
(9) Ara, I.; Forniés, J.; Fortuño, C.; Ibáñez, S.; Martín, A.; Mastrorilli, P.; Gallo, V. *Inorg. Chem.* **2008**, *47*, 9069–9080.
(10) Alonso, E.; Casas, J. M.; Cotton, F. A.; Feng, X. J.; Forniés, J.; Fortuño, C.; Tomás, M. *Inorg. Chem.* **1999**, *38*, 5034–5040.
(11) Alonso, E.; Casas, J. M.; Forniés, J.; Fortuño, C.; Martín, A.; Orpen, A. G.; Tsipis, C. A.; Tsipis, A. C. *Organometallics* **2001**, *20*, 5571–5582.

Published on Web 12/08/2010

Scheme 1

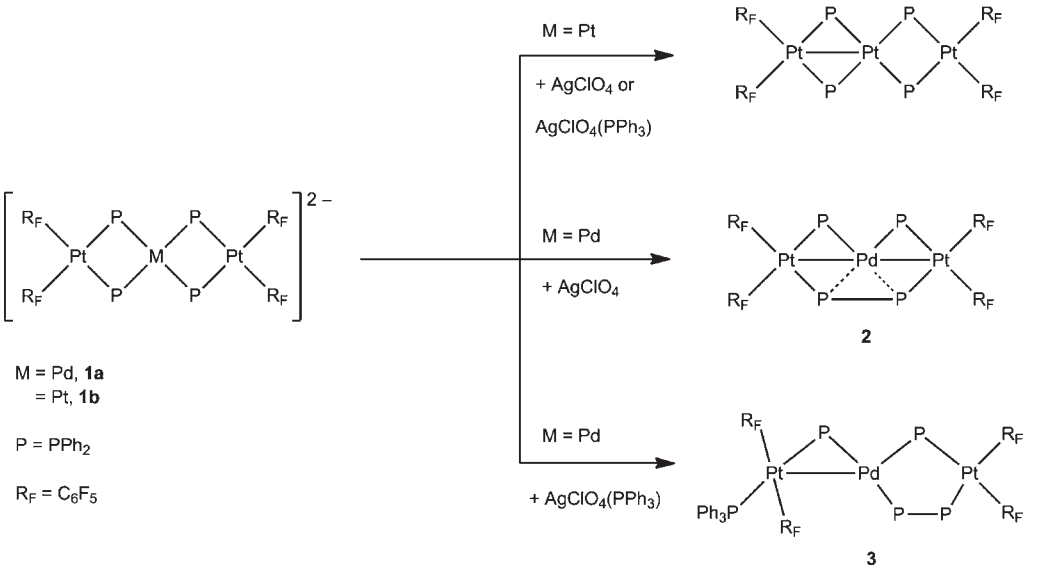

In one of our laboratories, we have found that the anionic trinuclear derivatives $[NBu_4]_2[(R_F)_2Pt(\mu\text{-}PPh_2)_2M(\mu\text{-}PPh_2)_2\text{-}Pt(R_F)_2]$ (M = Pt, Pd; $R_F = C_6F_5$) react with 2 equiv of $AgClO_4$ to afford Ag^0 and the 46e complexes $[(R_F)_2Pt^{III}(\mu\text{-}PPh_2)_2M^{III}(\mu\text{-}PPh_2)_2Pt^{II}(R_F)_2]$ (Scheme 1). For M = Pt, (**1b**) the complex with two Pt^{III} centers, $[(R_F)_2Pt^{III}(\mu\text{-}PPh_2)_2Pt^{III}(\mu\text{-}PPh_2)_2Pt(R_F)_2]$, was stable[11] but when M was Pd, the analogous $Pt^{III}-Pd^{III}$ complex could not be isolated since it quickly evolved through an unprecedented reductive coupling of two phosphanido bridged ligands, into the 44e complex $[(R_F)_2Pt^{II}(\mu\text{-}PPh_2)Pd^{II}(\mu\text{-}PPh_2)(\mu\text{-}Ph_2P\text{-}PPh_2)Pt^{II}\text{-}(R_F)_2]$ (**2**) (Scheme 1).[13]

In this paper we report on the reactions of $[NBu_4]_2\text{-}[(R_F)_2Pt(\mu\text{-}PPh_2)_2Pd(\mu\text{-}PPh_2)_2Pt(R_F)_2]$ (**1a**) with $[AgOClO_3\text{-}(PPh_3)]$ or with $AgClO_4$ and $PEtPh_2$, which resulted in the oxidation of the two bridging diphenylphosphanides to give the 46e species $[(PPh_3)(C_6F_5)_2Pt(\mu\text{-}PPh_2)Pd(\mu\text{-}PPh_2)(\mu\text{-}Ph_2P\text{-}PPh_2)Pt(C_6F_5)_2]$ (**3**) and $[(PEtPh_2)(C_6F_5)_2Pt(\mu\text{-}PPh_2)Pd(\mu\text{-}PPh_2)(\mu\text{-}Ph_2P\text{-}PPh_2)Pt(C_6F_5)_2]$ (**4**), respectively. Both species are characterized by a complex dynamic behavior in solution, which is the result of several independent processes imputable to steric and electronic effects.

The synthesis and the structural properties of the related complexes $[(CO)(C_6F_5)_2Pt(\mu\text{-}PPh_2)Pd(\mu\text{-}PPh_2)(\mu\text{-}Ph_2P\text{-}PPh_2)\text{-}Pt(C_6F_5)_2]$ (**6**, 46e), $[(py)(C_6F_5)_2Pt(\mu\text{-}PPh_2)Pd(\mu\text{-}PPh_2)(\mu\text{-}Ph_2P\text{-}PPh_2)Pt(C_6F_5)_2]$ (**7**, 46e), $[(PEtPh_2)(C_6F_5)_2Pt(\mu\text{-}PPh_2)\text{-}Pd(\mu\text{-}PPh_2)(CH_3CN)(\mu\text{-}Ph_2P\text{-}PPh_2)Pt(C_6F_5)_2]$ (**8**, 48e), and $[(CO)(C_6F_5)_2Pt(\mu\text{-}PPh_2)Pd(\mu\text{-}PPh_2)(\mu\text{-}Ph_2P\text{-}PPh_2)Pt(C_6F_5)_2]$ (**9**, 48e) are also discussed.

Results and Discussion

While the reaction of the *homo*trinuclear complex $[NBu_4]_2[(R_F)_2Pt(\mu\text{-}PPh_2)_2Pt(\mu\text{-}PPh_2)_2Pt(R_F)_2]$ (**1b**) with $[Ag(OClO_3)(PPh_3)]$ gave the same outcome achieved using $AgClO_4$, that is, the formation of $[(R_F)_2Pt^{III}(\mu\text{-}PPh_2)_2Pt^{III}(\mu\text{-}PPh_2)_2Pt^{II}(R_F)_2]$[11] (Scheme 1), when the *hetero*trinuclear complex $[NBu_4]_2[(R_F)_2Pt(\mu\text{-}PPh_2)_2Pd(\mu\text{-}PPh_2)_2Pt(R_F)_2]$ (**1a**) was reacted with $[Ag(OClO_3)(PPh_3)]$, (or with $AgClO_4$ and PPh_3 with **1a**/$AgClO_4$/PPh_3 in 1:2:1 molar ratio), the new 46e complex $[(PPh_3)(R_F)_2Pt(\mu\text{-}PPh_2)Pd(\mu\text{-}PPh_2)(\mu\text{-}Ph_2P\text{-}PPh_2)\text{-}Pt(R_F)_2]$ (**3**) formed (Scheme 2), along with Ag^0. Complex **3** was also obtained by reacting **2** with 1 equiv PPh_3 (Scheme 2), thus paving the way to the synthesis of other heterotrinuclear clusters analogous to **3** but having a different terminal ligand bound to Pt.[2]

The crystal structure of complex **3** has been determined by X-ray diffraction methods and is shown in Figure 1. Crystal data and other details of the structure analyses are reported in Table 1. Selected bond distances and angles are shown in Table 2. Complex **3** can be considered to be formed by two fragments, "$Pd(\mu\text{-}P(1)Ph_2)(\mu\text{-}Ph_2P\text{-}PPh_2)Pt(1)(C_6F_5)_2$" and "*trans*-$Pt(2)(C_6F_5)_2(PPh_3)$", connected by the $\mu\text{-}P(2)Ph_2$ ligand. The Pt(1)−Pd separation is 3.990(1) Å, excluding any intermetallic interaction. The Pt(1) center shows a square planar coordination geometry with the C_6F_5 rings almost perpendicular to the coordination plane. The dihedral angle formed by the best Pt(1) square plane and the plane defined by Pd and the phosphorus atoms bonded to it is 33.4(1)°. The angles around palladium are 101.2(1)°, 91.5(1)°, and 166.6(2)°. The Pd and Pt(2) atoms are single-bridged by the $P(2)Ph_2$ ligand and connected by a rather long (3.237(1) Å) dative Pt(2)−Pd bond which saturates the electronic demand of Pd. Although the Pt(2)−Pd distance is longer than those found so far for related $\mu\text{-}PPh_2$−Pd-Pt rings,[12,13] the existence of the Pt(2)−Pd bond is confirmed by the low field resonance of the ^{31}P NMR chemical shift of the bridging phosphanide ($\delta_{P(2)} =$ 121) observed both in solution and in the solid state which strongly support the existence of a three-membered Pt−Pd−P ring. Such a chemical shift is in the range expected for ^{31}P nuclei of phosphanido groups in the fragment $M(\mu\text{-}PPh_2)M$ with an M−M bond.[14−18] In agreement with this, the presence of (poorly resolved) ^{195}Pt satellites because of the coupling of P(1) with $^{195}Pt(2)$ in the $^{31}P\{^1H\}$ NMR spectrum

(12) Forniés, J.; Fortuño, C.; Ibáñez, S.; Martín, A. *Inorg. Chem.* **2008**, *47*, 5978–5987.
(13) Forniés, J.; Fortuño, C.; Ibáñez, S.; Martín, A.; Tsipis, A. C.; Tsipis, C. A. *Angew. Chem., Int. Ed.* **2005**, *44*, 2407–2410.
(14) Alonso, E.; Forniés, J.; Fortuño, C.; Martín, A.; Orpen, A. G. *Organometallics* **2000**, *19*, 2690–2697.
(15) Falvello, L. R.; Forniés, J.; Fortuño, C.; Martín, A.; Martínez-Sariñena, A. P. *Organometallics* **1997**, *16*, 5849–5856.

Scheme 2

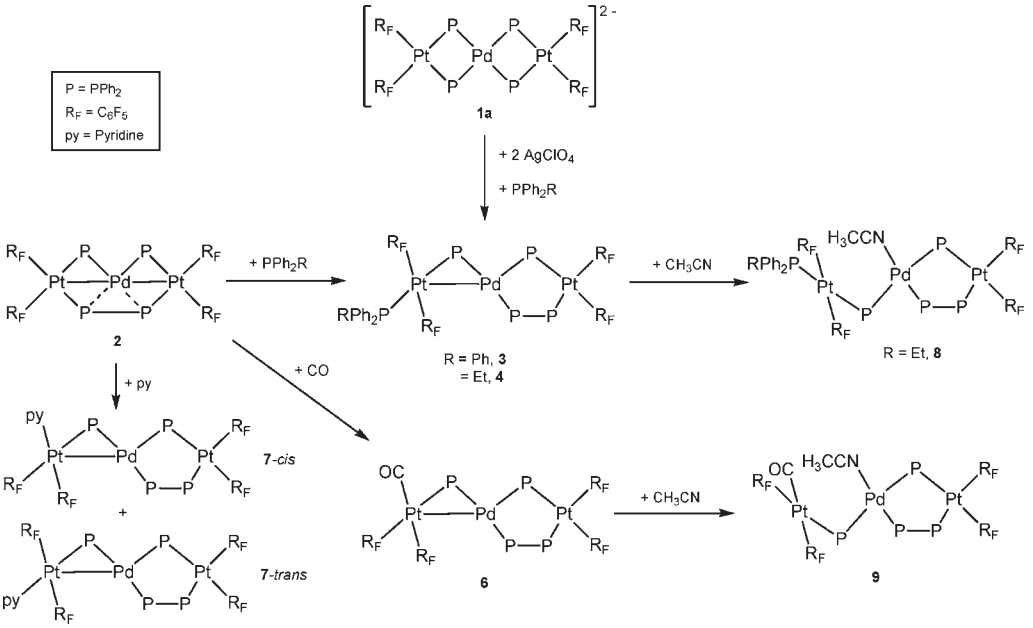

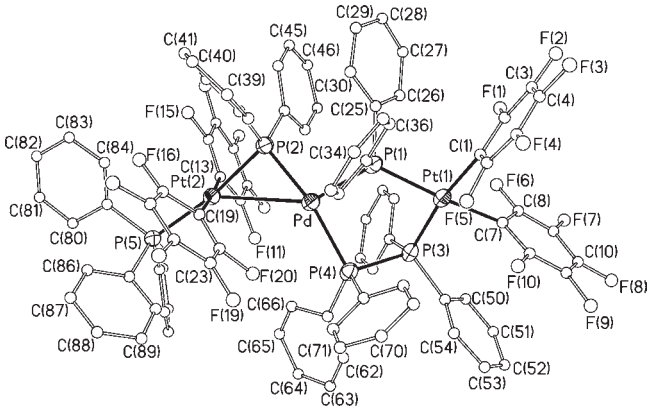

Figure 1. Molecular structure of complex $[(PPh_3)(R_F)_2Pt(\mu\text{-}PPh_2)Pd(\mu\text{-}PPh_2)(\mu\text{-}Ph_2P\text{-}PPh_2)Pt(R_F)_2]$ (**3**).

at low temperature further confirms the existence of the Pt(2)−Pd bond.[14,16,17,19]

The NMR and XRD data of systems displaying Pd-μ-PPh_2-Pt moieties, with or without metal−metal bond, that buttress the existence of the Pt(2)-Pd bond in complex **3** are collected in Table 3. A cause for the long value of the Pt(2)−Pd bond length may reside in the steric crowding around the three-membered Pt(2)−Pd−P ring, which prevents the metal centers from approaching closer each other. Such a steric crowding could also, on one hand account for the observed stability of complex **3** toward the addition of relatively bulky ligands, such as free PPh_3; on the other hand it could explain the dynamic behavior exhibited by **3** in solution (vide infra). The relative disposition of the two pentafluorophenyl groups in mutually trans position is presumably also a consequence of steric requirements which force the bulkiest ligand around Pt^2 to stay trans to μ-P^2. In fact, the related heterotrinuclear complex $[(CH_3CN)(R_F)_2Pt^2(\mu\text{-}PPh_2)Pd(\mu\text{-}PPh_2)(\mu\text{-}Ph_2P\text{-}PPh_2)Pt^1(R_F)_2]$ (**5**)[12] having the less sterically demanding CH_3CN in place of PPh_3 (i) displays the C_6F_5 groups bonded to Pt^2 in mutually *cis* position; (ii) shows a significantly shorter Pt^2−Pd bond distance [2.885(1) Å].

To confirm the role of steric effects of ligand L in complexes of general formula $[(L)(R_F)_2Pt^2(\mu\text{-}PPh_2)Pd(\mu\text{-}PPh_2)(\mu\text{-}Ph_2P\text{-}PPh_2)Pt^1(R_F)_2]$, we have chosen three ligands L of different bulkiness such as PPh_2Et, pyridine and CO and we have prepared the new heterotrinuclear species **4** (L = PPh_2Et), **6** (L = CO) and **7** (L = py). Complex **4** was prepared by treating **1a** with PPh_2Et and 2 equiv $AgClO_4$[21] while **6** and **7** were obtained by exposing **2** to one atmosphere of CO or to an excess of pyridine, respectively.

Although the crystals of **4** were not suitable for XRD analysis, NMR spectroscopy revealed that its structure is identical to that of complex **3**, the only difference being the terminal PPh_2Et in place of PPh_3. In the case of **4** the signal of the bridging phosphanide μ-P(2) falls at δ 121.0, confirming the presence of the Pt(2)-Pd bond, and the position of PPh_2Et *trans* to μ-P(2) is ascertained by the $^2J_{P5,P2}$ of 285 Hz (the $^2J_{P5,P2}$ for **3** is 290 Hz). The similarity between **4** and **3** extends also to the lack of reaction of **4** with excess of the bulky phosphane PPh_2Et.

As far as the carbonyl complex **6** is concerned, its crystal structure has been determined by X-ray diffraction methods and is shown in Figure 2. Crystal data and other details of the structure analyses are reported in Table 1. Selected bond distances and angles are shown in Table 4. It is apparent that in this case, as expected in the light of the small size of CO, the two pentafluorophenyl groups bonded to Pt(2) are located mutually cis, while in **3** and **4** the C_6F_5 groups are mutually

(16) Alonso, E.; Forniés, J.; Fortuño, C.; Martín, A.; Orpen, A. G. *Organometallics* **2001**, *20*, 850–859.
(17) Forniés, F.; Fortuño, C.; Ibáñez, S.; Martín, A. *Inorg. Chem.* **2006**, *45*, 4850–4858.
(18) Mastrorilli, P. *Eur. J. Inorg. Chem.* **2008**, 4835–4850.
(19) Forniés, J.; Fortuño, C.; Gil, R.; Martín, A. *Inorg. Chem.* **2005**, *44*, 9534–9541.
(20) Maassarini, F.; Davidson, M. F.; Wehman-Ooyevaar, C. M.; Grove, D. M.; van Koten, M. A.; Smeets, W. J. J.; Spek, A. L.; van Koten, G. *Inorg. Chim. Acta* **1995**, *235*, 327–338.

(21) Complex **4** was also obtained by reaction of **2** with $PEtPh_2$.

Table 1. Crystal Data and Structure Refinement for Complexes $[(PPh_3)(R_F)_2Pt(\mu\text{-}PPh_2)Pd(\mu\text{-}PPh_2)(\mu\text{-}Ph_2P\text{-}PPh_2)Pt(R_F)_2]\cdot CH_2Cl_2$ (**3**·CH_2Cl_2), $[(CO)(R_F)_2Pt(\mu\text{-}PPh_2)Pd(\mu\text{-}PPh_2)(\mu\text{-}Ph_2P\text{-}PPh_2)Pt(R_F)_2]\cdot 0.75n\text{-}C_6H_{14}\cdot 0.2CH_2Cl_2$ (**6**·$0.75n$-C_6H_{14}·$0.2CH_2Cl_2$), $[(py)(R_F)_2Pt(\mu\text{-}PPh_2)Pd(\mu\text{-}PPh_2)(\mu\text{-}Ph_2P\text{-}PPh_2)Pt(R_F)_2]$ (**7***-trans*), and $[(py)(R_F)_2Pt(\mu\text{-}PPh_2)Pd(\mu\text{-}PPh_2)(\mu\text{-}Ph_2P\text{-}PPh_2)Pt(R_F)_2]\cdot 1.4CH_2Cl_2$ (**7***-cis*·$1.4CH_2Cl_2$)

	3·CH_2Cl_2	**6**·$0.75n$-C_6H_{14}·$0.2CH_2Cl_2$	***7trans***	***7cis***·$1.4CH_2Cl_2$
formula	$C_{90}H_{55}F_{20}P_5PdPt_2\cdot CH_2Cl_2$	$C_{73}H_{40}F_{20}P_4OPdPt_2\cdot 0.75n\text{-}C_6H_{14}\cdot 0.2CH_2Cl_2$	$C_{77}H_{45}F_{20}NP_4PdPt_2$	$C_{77}H_{45}F_{20}NP_4PdPt_2\cdot 1.4CH_2Cl_2$
M_t [g mol^{-1}]	2252.70	2015.12	1984.60	2103.50
T [K]	173(1)	100(1)	123(1)	100(1)
λ [Å]	0.71073	0.71073	0.71073	0.71073
crystal system	monoclinic	triclinic	monoclinic	triclinic
space group	$P2_1$	P-1	$P2_1/c$	P-1
a [Å]	12.6057(6)	11.8043(1)	17.6125(6)	12.8636(8)
b [Å]	20.2225(10)	15.666(3)	22.1870(7)	13.7681(9)
c [Å]	16.4417(8)	21.543(4)	18.1842(6)	21.462(3)
α [deg]	90	95.649(3)	90	82.987(8)
β [deg]	90.328(1)	96.502(3)	104.197(3)	78.649(8)
γ [deg]	90	108.579(3)	90	81.836(5)
V [Å^3]	4191.2(4)	3713.5(11)	6888.8(4)	3671.5(6)
Z	2	2	4	2
ρ [g cm^{-3}]	1.785	1.802	1.914	1.903
μ [mm^{-1}]	3.793	4.193	4.504	4.330
F(000)	2188	1948	3824	2030
2θ range [deg]	3.2−50.3	3.1−50.1	7.8−50.1	7.5−50.2
no. of reflns collected	23 163	20 596	32 559	39 047
no. of unique reflns	14 214	12 951	12 153	12 919
R(int)	0.1283	0.0341	0.0313	0.0307
final R indices [$I > 2\sigma(I)$][a]				
R_1	0.0729	0.0467	0.0392	0.0324
R_2	0.1724	0.1106	0.0832	0.0777
R indices (all data)				
R_1	0.0869	0.0614	0.0479	0.0473
R_2	0.1831	0.1181	0.0871	0.0853
abs str param	−0.004			
GOF on F^2[b]	1.006	1.058	1.088	1.032

[a] $R_1 = \sum(|F_o| - |F_c|)/\sum|F_o|$. $R_2 = [\sum w(F_o^2 - F_c^2)^2/\sum w(F_o^2)^2]^{1/2}$. [b] GOF $= [\sum w\,(F_o^2 - F_c^2)^2/(n_{obs} - n_{param})]^{1/2}$.

Table 2. Selected Bond Distances (Å) and Angles (deg) for $[(PPh_3)(R_F)_2Pt(\mu\text{-}PPh_2)Pd(\mu\text{-}PPh_2)(\mu\text{-}Ph_2P\text{-}PPh_2)Pt(R_F)_2]\cdot CH_2Cl_2$ (**3**·CH_2Cl_2)

Pt(1)−C(7)	2.071(18)	Pt(1)−C(1)	2.095(14)	Pt(1)−P(3)	2.288(4)
Pt(1)−P(1)	2.377(4)	Pt(2)−C(13)	2.078(17)	Pt(2)−C(19)	2.111(15)
Pt(2)−P(2)	2.364(4)	Pt(2)−P(5)	2.366(4)	Pt(2)−Pd	3.2370(14)
Pd−P(2)	2.272(4)	Pd−P(1)	2.321(4)	Pd−P(4)	2.418(4)
P(1)−C(31)	1.849(18)	P(1)−C(25)	1.851(16)	P(2)−C(37)	1.78(2)
P(2)−C(43)	1.843(19)	P(3)−C(55)	1.823(18)	P(3)−C(49)	1.863(16)
P(3)−P(4)	2.240(6)				
C(7)−Pt(1)−C(1)	85.9(6)	C(7)−Pt(1)−P(3)	88.0(5)
C(1)−Pt(1)−P(3)	169.9(5)	C(7)−Pt(1)−P(1)	176.4(5)
C(1)−Pt(1)−P(1)	92.1(4)	P(3)−Pt(1)−P(1)	94.39(15)
C(13)−Pt(2)−C(19)	176.2(7)	C(13)−Pt(2)−P(2)	89.6(4)
C(19)−Pt(2)−P(2)	90.0(5)	C(13)−Pt(2)−P(5)	90.6(4)
C(19)−Pt(2)−P(5)	89.2(5)	P(2)−Pt(2)−P(5)	171.61(14)
C(13)−Pt(2)−Pd	104.0(4)	C(19)−Pt(2)−Pd	78.3(4)
P(2)−Pt(2)−Pd	44.55(10)	P(5)−Pt(2)−Pd	143.12(10)
P(2)−Pd−P(1)	101.20(15)	P(2)−Pd−P(4)	166.57(16)
P(1)−Pd−P(4)	91.45(14)	P(2)−Pd−Pt(2)	46.89(11)
P(1)−Pd−Pt(2)	147.97(11)	P(4)−Pd−Pt(2)	120.58(11)

trans. The lesser sterical hindrance of the CO compared to PPh_3 results also in a shorter Pt(2)−Pd distance, 2.862(1) Å, than the analogous one in **3** (3.237(1) Å). The fragment "$Pd(\mu\text{-}PPh_2)(\mu\text{-}Ph_2P\text{-}PPh_2)Pt(1)(C_6F_5)_2$" is very similar to the analogous one described for **3**. The Pt(1)−Pd distance is 3.973(1) Å (cf., 3.990(1) Å in **3**) excluding any interaction between these centers. The three metal centers lie in a nearly linear array, with a Pt(1)−Pd−Pt(2) angle of 167.3(1)° (cf., 165.7(1)° Å in **3**).

NMR Studies. The $^{31}P\{^1H\}$ NMR spectra of **3** and **4** at room temperature are almost superimposable, and show broad peaks as a consequence of dynamic processes occurring in the molecules (Figure 3a). However, on lowering the temperature down to 213 K, the dynamic processes involving the P atoms were blocked and the signals in the $^{31}P\{^1H\}$ NMR spectrum became sharp (Figure 3b).

At 213 K, the chemical shift of the P(2) atoms falls at δ 121 for both **3** and **4**, the signals of the phosphanido P(1) not subtending any metal−metal bond falls at δ 47 for **3** and at δ 45 for **4**, the P(5) signals of the terminal phosphanes were found at δ 18 for **3** and δ 16 for **4**, while the ^{31}P chemical shifts of the coordinated tetraphenyldiphosphane were δ(P3) 45, δ(P4) 71 for **3** and δ(P3) 41, δ(P4) 67 for **4**.

In the $^{31}P\{^1H\}$ NMR spectra at low T, the signals due to P(4) for **3** and **4** appear as doublets of doublets of doublets with coupling constants values of ∼270, 180, and 55 Hz.

The larger values are ascribed to the coupling with P(2) and P(3) respectively, while the 55 Hz value, which does not appear in any of the other ^{31}P signal, must be attributed to a heterocoupling. In order to identify the nucleus scalar coupled to P(4), we have recorded a ^{31}P NMR spectrum under selective ^{19}F decoupling as well as a $^{19}F-^{31}P$ HMQC experiment that indicated that P(4) is scalar coupled to F(20) (see Figure 1 for the numbering of F atoms), the most deshielded ^{19}F nucleus ($\delta F(20) = -98.0$ for **3** and -99.4 for **4**, vide infra). In fact the $^{31}P\{^{19}F\}_{sel}$ NMR recorded under selective irradiation of F(20) resulted in a P(4) signal simplified into a doublet of doublets ($\sim$270 and 180 Hz). Accordingly, the $^{19}F-^{31}P$ HMQC spectrum of **4** (Figure 4) showed an intense cross peak between P(4) and F(20). A closer inspection of the $^{19}F-^{31}P$ HMQC spectrum reveals correlations between P(1) and F(6) and between P(1) and F(10). Such weak cross peaks are due to scalar couplings through four bonds and the relevant coupling constants are too small to be extracted from the 1D ^{19}F or ^{31}P NMR spectra.

Table 3. XRD and ^{31}P NMR Features of Systems Displaying Pd$-\mu$-PPh$_2-$Pt Moieties

complex	$\delta_{\mu-P}$	d_{Pt-Pd} (Å)	Pt−Pd bond	ref.
2	120	2.89	yes	13
5	145	2.89	yes	12
6	150	2.86	yes	this work
7-*cis*	153	2.98	yes	this work
7-*trans*	106	3.06	yes	this work
3	121	3.23	yes	this work
[(NCN)Pt(μ-PPh$_2$)Pd(H$_2$O)L]$^{+a}$	43	3.88	no	20
9	−10	4.17	no	this work
8	5	4.09	no	this work

^{a} L = (C$_6$H$_4$CH$_2$NMe$_2$-2); NCN = C$_6$H$_3$(CH$_2$NMe$_2$)$_2$-2,6.

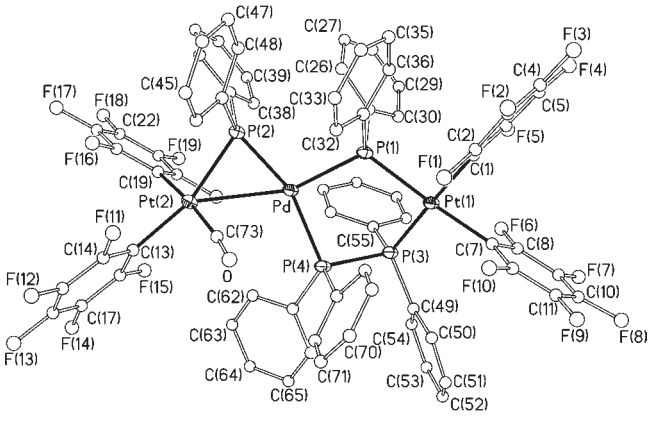

Figure 2. Molecular structure of complex [(CO)(R$_F$)$_2$Pt(μ-PPh$_2$)Pd-(μ-PPh$_2$)(μ-Ph$_2$P-PPh$_2$)Pt(R$_F$)$_2$] (**6**).

Long-range $^{19}F-X$ coupling constants have been reported for X = H,[22−28] C,[22] N,[29,30] F,[27,31−33] P,[34−37] and Pt,[38] and in most cases, they have been attributed to the so-called "through space" spin−spin coupling. Given that P(4) and F(20) are separated by five bonds, and in the light of the favorable spatial disposition (the P(4)−F(20) distance is 3.040 Å while the sum of the P and F van der Waals radii is 3.3 Å), the P(4)−F(20) coupling of ca. 55 Hz has to be assigned to a "through space" $^{19}F-^{31}P$ spin−-spin coupling. It is well-known that "through space" coupling derives from overlap interactions between filled orbitals that result in a no net bonding providing, nevertheless, an adequate pathway for transmitting spin information between the coupled nuclei. The theory originally developed for "through space" $^{19}F-^{19}F$ couplings (based on lone pair overlaps)[39,40] has been recently extended to "through space" $^{31}P-^{31}P$ couplings observed in transition metal complexes[41] by admitting that the transmission of spin information can occur via interaction between a lone pair and a bonding electron pair. In our case, the "through space" $^{19}F-^{31}P$ coupling can be ascribed to the interaction between a F(20) lone pair and the P(4)-Pd σ orbital (Figure 5).

The ^{19}F NMR spectrum of **3** (and **4**) at 298 K showed in the *ortho*-F region ($-90 \div -120$ ppm for these systems) a broad signal at δ −115.7 ppm for **3** (δ −116.0 ppm for **4**) flanked by ^{195}Pt satellites ($^3J_{F,Pt}$ = 282 Hz for **3** and $^3J_{F,Pt}$ = 291 Hz for **4**) and an extremely broad signal at δ apprximately −111 for both **3** and **4**, which barely emerges from the baseline. On lowering the temperature down to 213 K, eight *ortho*-^{19}F signals appear, indicating that at low T the *ortho*-F are all chemically inequivalent, due to a hindered rotation about the $C_{ipso}-Pt$ bonds.

For the more soluble complex **4**, the ^{19}F EXSY spectrum at 213 K is reported in Figure 6. It is apparent that, of the eight ^{19}F nuclei, the four more deshielded ones exchange between themselves (but not with the other four), while the remaining four ^{19}F nuclei (one of which is isochronous with one of the first group) are involved in two separate exchanges (see inset of Figure 6). The ^{19}F EXSY data can be explained by admitting that the four high-field *ortho*-F signals at δ −116.5, δ −116.2, δ −115.7, δ −115.4 belong to the C$_6$F$_5$ rings bonded to Pt(1) (rings A and B in Figure 7), while the low-field *ortho*-F signals at

Table 4. Selected Bond Distances (Å) and Angles (deg) for [(CO)(R$_F$)$_2$Pt(μ-PPh$_2$)Pd(μ-PPh$_2$)(μ-Ph$_2$P-PPh$_2$)Pt(R$_F$)$_2$]·0.75*n*-C$_6$H$_{14}$·0.2CH$_2$Cl$_2$ (**6**·0.75*n*-C$_6$H$_{14}$·0.2CH$_2$Cl$_2$)

Pt(1)−C(1)	2.048(8)	Pt(1)−C(7)	2.059(8)	Pt(1)−P(3)	2.270(2)
Pt(1)−P(1)	2.341(2)	Pt(2)−C(73)	1.929(9)	Pt(2)−C(19)	2.053(8)
Pt(2)−C(13)	2.073(8)	Pt(2)−P(2)	2.369(2)	Pt(2)−Pd	2.8621(8)
Pd−P(2)	2.220(2)	Pd−P(1)	2.340(2)	Pd−P(4)	2.363(2)

C(1)−Pt(1)−C(7)	85.3(3)	C(1)−Pt(1)−P(3)	176.6(2)
C(7)−Pt(1)−P(3)	92.9(2)	C(1)−Pt(1)−P(1)	90.9(2)
C(7)−Pt(1)−P(1)	176.2(2)	P(3)−Pt(1)−P(1)	90.91(7)
C(73)−Pt(2)−C(19)	175.1(3)	C(73)−Pt(2)−C(13)	88.2(3)
C(19)−Pt(2)−C(13)	86.9(3)	C(73)−Pt(2)−P(2)	97.3(2)
C(19)−Pt(2)−P(2)	87.5(2)	C(13)−Pt(2)−P(2)	164.2(2)
C(73)−Pt(2)−Pd	69.3(3)	C(19)−Pt(2)−Pd	114.7(2)
C(13)−Pt(2)−Pd	145.9(2)	P(2)−Pt(2)−Pd	49.12(5)
P(2)−Pd−P(1)	105.51(7)	P(2)−Pd−P(4)	160.10(8)
P(1)−Pd−P(4)	94.37(7)	P(2)−Pd−Pt(2)	53.78(5)
P(1)−Pd−Pt(2)	158.63(5)	P(4)−Pd−Pt(2)	106.35(5)

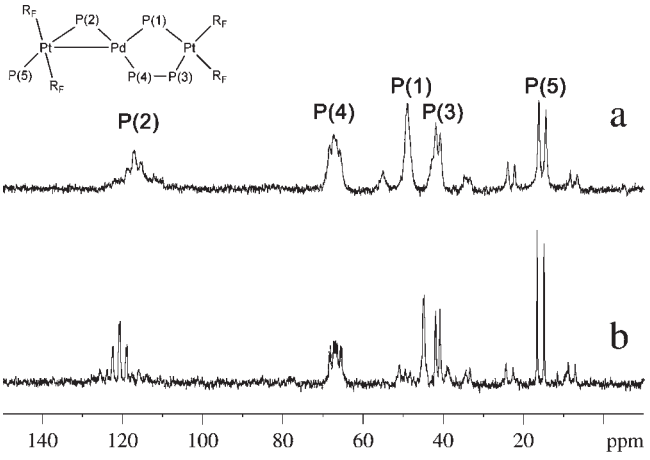

Figure 3. $^{31}P\{^{1}H\}$ NMR spectrum of **4** in $CDCl_3$: (a) at 298 and (b) 213 K.

δ −99.3, δ −111.0, δ −114.4, δ −115.4, belong to the C_6F_5 rings bonded to Pt(2) (rings C and D in Figure 7). The ^{19}F at δ −116.5 and one of those at δ −115.4 can be safely assigned to F(6) and F(10) of ring A, on the basis of the observed correlation between them and the P(1) in the $^{19}F-^{31}P$ HMQC spectrum (Figure 4). Thus, the signals at δ −116.2 and δ −115.7, which exchange between themselves but not with any other ^{19}F atom, must belong to F(1) and F(5) of ring B.

The cross peaks among the ^{19}F signals of rings C and D in the ^{19}F EXSY spectrum indicate an interchange process

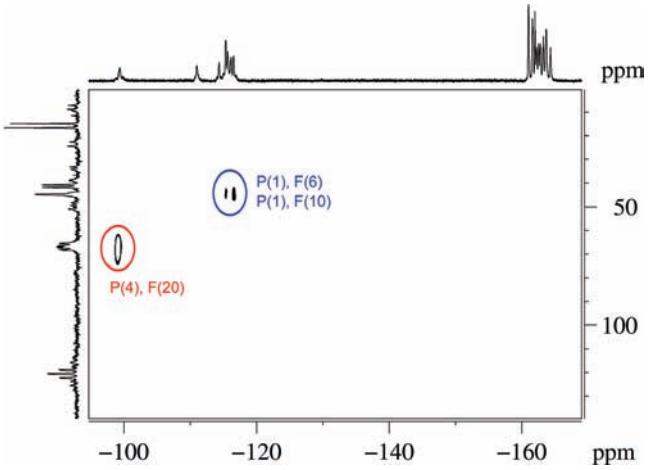

Figure 4. $^{19}F-^{31}P$ HMQC spectrum of **4** ($CDCl_3$, 213 K).

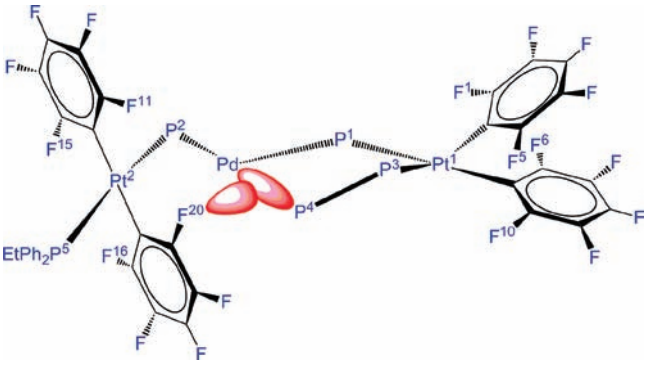

Figure 5. Overlap of filled orbitals responsible for the through-space F(20)−P(4) spin−spin coupling.

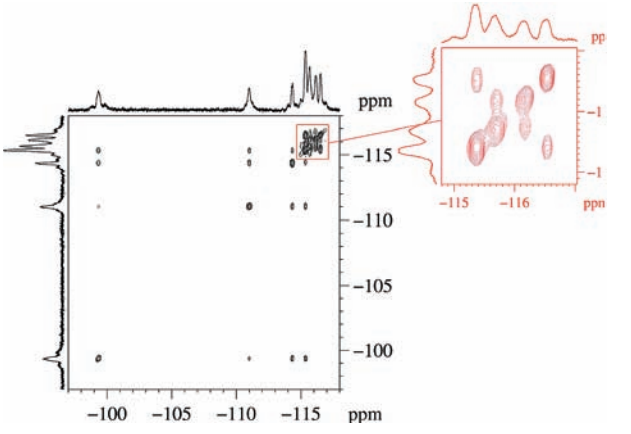

Figure 6. ^{19}F EXSY spectrum of **4** ($CDCl_3$, 213 K).

involving all of the four ^{19}F nuclei and not two ^{19}F couples separately, as in the case of rings A and B. This finding can be explained by admitting that, beside the rotation of rings C and D about the C−Pt bonds (responsible for the F(16)/F(20) and F(11)/ F(15) exchanges), another dynamic process must be operative. Such a process does not interchange any of the P atoms, as ascertained by a ^{31}P EXSY experiment at 213 K. A plausible process that can explain such data is the swinging of the P(3)−P(4) vector around its central point, the P(4) atom being above or below the Pd−P(1)−Pt(1)

(22) Crespo, M.; Solans, X.; Font-Bardía, M. *Organometallics* **1995**, *14*, 355–364.
(23) Leblanc, J. C.; Moïse, C. *Org. Magn. Reson.* **1980**, *14*, 157–160.
(24) Green, M. L. H.; Lindsell, W. E. *J. Chem. Soc. A* **1969**, 2215–2218.
(25) Bennett, R. L.; Bruce, M. I.; Gardner, R. C. F. *J. Chem. Soc., Dalton Trans.* **1973**, 2653–2657.
(26) Mallory, F. B.; Mallory, C. W.; Ricker, W. M. *J. Am. Chem. Soc.* **1975**, *97*, 4770–4771.
(27) Mallory, F. B.; Mallory, C. W.; Ricker, W. M. *J. Org. Chem.* **1985**, *50*, 457–461.
(28) Peris, E.; Lee, J. C., Jr.; Crabtree, R. H. *J. Chem. Soc., Chem. Commun.* **1994**, 2573–2573.
(29) Mallory, F. B.; Mallory, C. W. *J. Am. Chem. Soc.* **1985**, *107*, 4816–4819.
(30) Mallory, F. B.; Luzich, E. D.; Mallory, C. W.; Carroll, P. J. *J. Org. Chem.* **1992**, *57*, 366–370.
(31) Mallory, F. B.; Mallory, C. W.; Fedarko, M.-C. *J. Am. Chem. Soc.* **1974**, *96*, 3536–3542 and refs therein.
(32) Albéniz, A. C.; Casado, A. L.; Espinet, P. *Organometallics* **1997**, *16*, 5416–5423.
(33) Mallory, F. B.; Mallory, C. W.; Baker, M. B. *J. Am. Chem. Soc.* **1990**, *112*, 2577–2581.
(34) Miller, G. R.; Jankowsky, A. W.; Grim, S. O. *J. Chem. Phys.* **1969**, *51*, 3185–3190.
(35) Barnes, N. A.; Brisdon, A. K.; Brown, F. R. W.; Cross, W. I.; Crossley, I. R.; Fish, C.; Morey, J. V.; Pritchard, R. G.; Sekhri, L. *New J. Chem.* **2004**, *28*, 828–837.
(36) Kruck, M.; Munoz, M. P.; Bishop, H. L.; Frost, C. G.; Chapman, C. J.; Kociok-Köhn, G.; Butts, C. P.; Lloyd-Jones, G. C. *Chem.—Eur. J.* **2008**, *14*, 7808–7812.
(37) Hughes, R. P.; Laritchev, R. B.; Williamson, A.; Incarvito, C. D.; Zakharov, L. N.; Rheingold, A. L. *Organometallics* **2002**, *21*, 4873–4885.
(38) Phillips, I. G.; Ball, R. G.; Cavell, R. G. *Inorg. Chem.* **1987**, *26*, 4074–4079.
(39) Mallory, F. B. *J. Am. Chem. Soc.* **1973**, *95*, 7747–7752.
(40) Mallory, F. B.; Mallory, C. W.; Butler, K. E.; Levis, M. B.; Xia, A. Q.; Luzik, E. D.; Fredenburgh, L. E.; Ramanjulu, M. M.; Van, Q. N.; Francl, M. M.; Fredd, D. A.; Wray, C. C.; C., H.; Nerz-Stormes, M.; Carroll, P. J.; Chirlian, L. E. *J. Am. Chem. Soc.* **2000**, *122*, 4108–4116.
(41) Hierso, J.-C.; Fihri, A.; Ivanov, V. V.; Hanquet, B.; Pirio, N.; Donnadieu, B.; Rebière, B.; Amardeil, R.; Meunier, P. *J. Am. Chem. Soc.* **2004**, *126*, 11077–11087.

plane, i. e. a puckering of the five membered ring takes place (Scheme 3). Thus the P(4) atom is alternatively closer to F(20) or F(11), resulting in their chemical exchange. At 320 K the ^{19}F NMR spectrum in the *ortho*-F region shows one broad signal at δ −115.9 ascribable to the almost isochronous *ortho*-F atoms of rings A and B, along with a very broad signal centered at δ −110.8 due to the *ortho*-F atoms of rings C and D.

Given that both Pt atoms in **4** are bonded to C_6F_5 groups, $^{19}F-^{195}Pt$ HMQC experiments were carried out to find the ^{195}Pt chemical shifts. However, even at low T (213 K) only the signal ascribable to Pt(2) was detected ($\delta_{Pt(2)}$ −4350), by spanning the −3000/−5000 ppm region.

In order to gain insights into the dynamic process responsible for the broadness of the ^{31}P NMR signals of **3** and **4** at 298 K, as well as of the *ortho*-^{19}F signals of rings C and D at 320 K, we carried out a ^{31}P EXSY study, which basically gave the same outcome for the two complexes. For the sake of brevity, we will describe in the following only the NMR study carried out on the more soluble species **4**.

The $^{31}P\{^1H\}$ EXSY spectrum of **4** recorded at 298 K in $CDCl_3$ with a mixing time of 100 ms is reported in Figure 8 and shows exchange cross peaks due to two independent processes, as indicated by the different intensities of such cross peaks. The most intense cross peaks, circled in red and related to the most frequent process, indicate a chemical exchange between P(3) and P(4), while the less intense cross peaks, (circled in green and related to a less frequent process), indicate a chemical exchange between P(2) and P(5).[42]

Recalling that at low T the swinging of the P(3)−P(4) vector around its central point was invoked to explain the ^{19}F EXSY spectrum, at higher temperatures it can be conceivable that such motion ends up in the rotation of the coordinated tetraphenyldiphosphane as shown in Scheme 4, accounting for the P3/P4 exchange in the $^{31}P\{^1H\}$ EXSY spectrum of **4**.

As far as the P(5)/P(2) exchange is concerned, a plausible mechanism explaining the experimental observation is outlined in Scheme 5. After Pt(2)−Pd bond breaking, the electron rich Pt(2) fragment might undergo oxidative

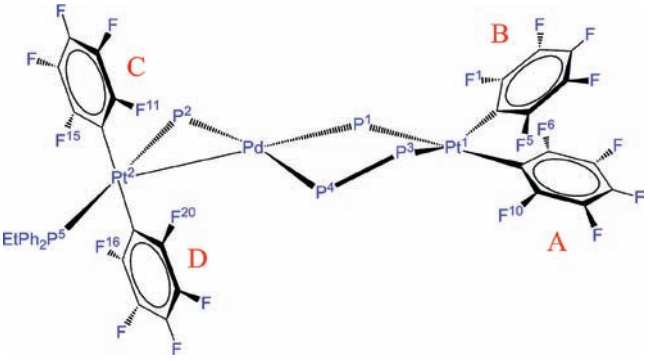

Figure 7. Sketch of complex **4** with labeled C_6F_5 rings.

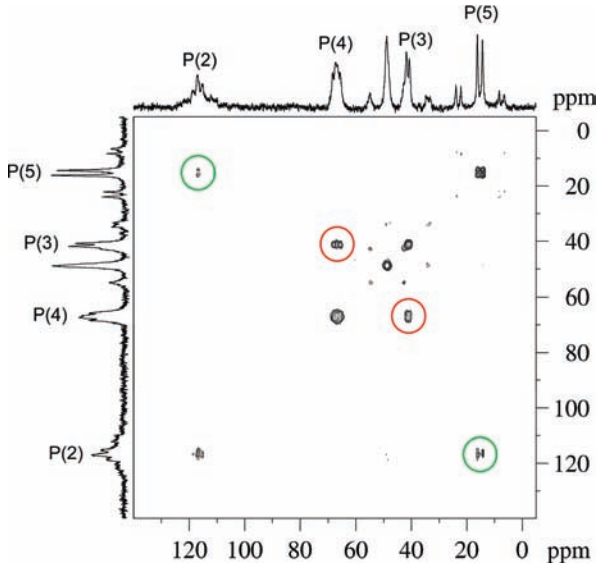

Figure 8. ^{31}P EXSY spectrum of **4** ($CDCl_3$, 298 K, τ_m = 100 ms).

Scheme 3

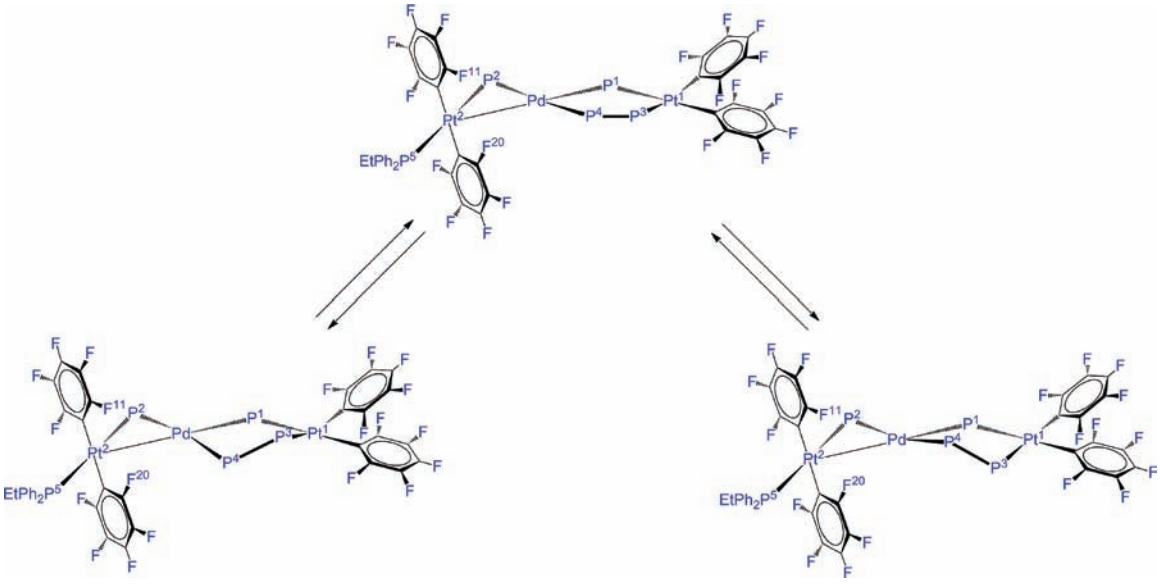

Scheme 4

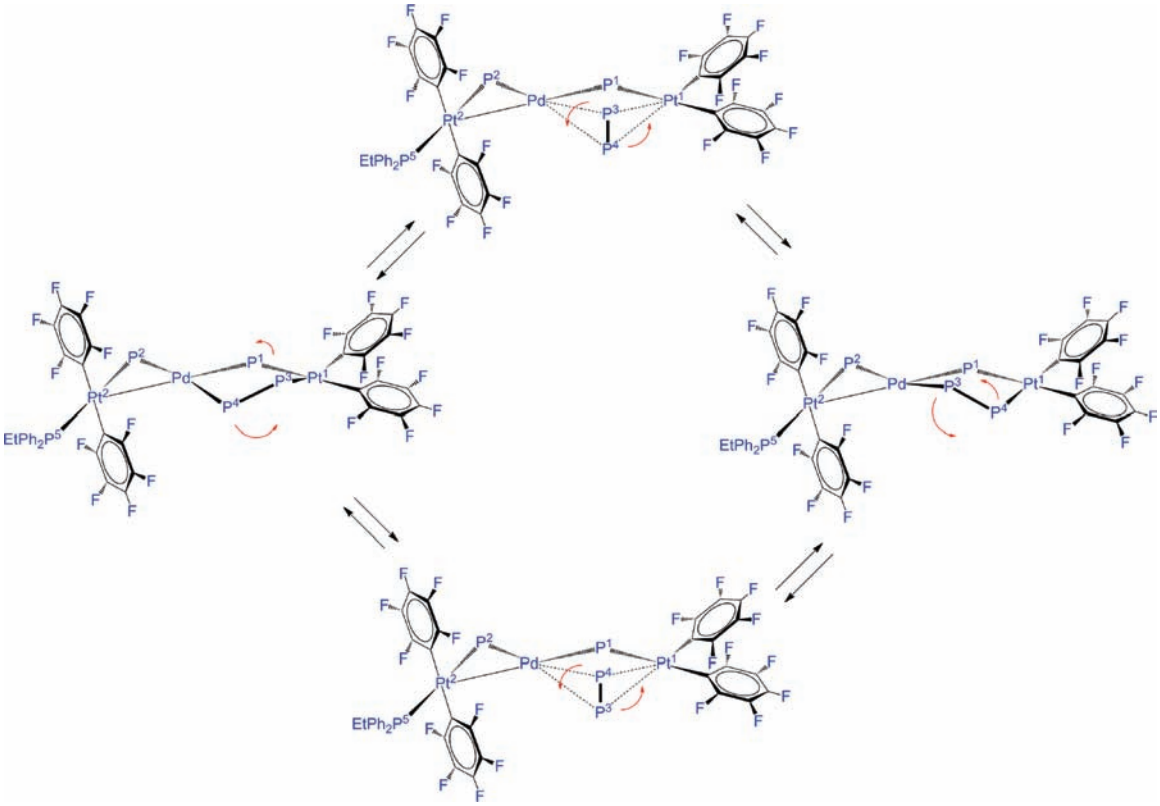

addition of the P−Et bond of the terminally bonded PPh_2Et ligand, forming the intermediate **E** in which the Pt(2) bears two C_6F_5, an ethyl group and is connected to Pd by two μ-PPh_2 bridges. The reformation of the P−Et bond involving the P atom originally bridging Pt(2) and Pd might be responsible for the observed P(2)/P(5) exchange. In the case of **3**, the P(5)/P(2) exchange is explained in terms of oxidative addition of a P(5)−Ph bond, followed by reductive elimination involving the phenyl and the $P(2)Ph_2$ groups.

We have ascertained by VT $^{31}P\{^1H\}$ NMR analysis that, in the case of **4**, the expected phenyl migration from P(5) to P(2) did not occur.[43] This uncommon behavior is intriguing in the light of the known superiority of the phenyl as migrating group with respect to alkyls.

In the $^{31}P\{^1H\}$ NMR spectrum of the carbonyl complex **6** at 293 K, the bridging phosphanido P(2) subtending the Pt(2)−Pd bond gives a very broad signal centered at δ 125, the phosphanido P(1) bridging Pd and Pt(1) gives a doublet at δ 53, while the tetraphenyldiphosphane P(3) and P(4) were found at δ 46 and δ 68, respectively. At 183 K, the chemical shifts of P(1) (δ 43), P(2) (δ 151), and P(4) (δ 59) signals significantly change and the signal due to P(2) becomes sharp.

The ^{19}F NMR spectrum at 293 K in the *ortho*-F region shows two sets of signals ascribed, one to the C_6F_5 rings bonded to Pt(2), and the other to the C_6F_5 rings bonded to Pt(1). Of these, one set of signals is very broad. The ^{19}F spectrum at 193 K shows sharp signals which give rise to a complex pattern due to the chemical unequivalence of all the fluorine atoms (at hindered rotation about the Pt−C_6F_5 bonds).

A possible explanation for the $^{31}P\{^1H\}$ and ^{19}F NMR data of **6** is that the structure found in the solid state is maintained at 193 K. On rising the temperature up to 293 K an isomerization at Pt(2) may occur, in which the pentafluorophenyl groups pass from mutually cis to mutually trans position. In keeping with this, the IR spectrum of **6** in solid state shows only one ν(C≡O) absorption (2087 cm^{-1}), while two ν(C≡O) absorptions (2095 and 2083 cm^{-1}) of similar intensity are observed in CH_2Cl_2 solution at 298 K. This behavior prompted us to study the reaction of complex **2** with pyridine, a ligand of bulkiness intermediate between CO and PPh_2R. The reaction of complex **2** with an excess of pyridine at room temperature yielded the complex $[(py)(R_F)_2Pt^2(\mu\text{-}PPh_2)\text{-}Pd(\mu\text{-}P^2Ph_2)(\mu\text{-}Ph_2P\text{-}PPh_2)Pt^1(R_F)_2]$ **7**. The crystallization method results in the isolation of a crop of pure **7*trans*** and, from the resulting mother liquors, a mixture of two isomers **7**-*trans* (the more important component) and **7**-*cis* were obtained. We have not been able to separate pure **7**-*cis* from the mixture. Fortunately, X-ray quality

(42) Although no precise assessment of the constant rate associated to the processes could be made, due to signal overlapping, the value of the P3/P4 exchange constant rate was found nearly twice the P2/P5 one. Moreover, in order to render the EXSY spectrum devoid of COSY artifacts [the couples P3/P4 (J = 178 Hz) and P5/P2 (J = 285 Hz) are strongly scalar coupled] the experiments were recorded using mixing time values higher than 100 ms. The above-mentioned absence of any cross peak in the ^{31}P EXSY spectrum recorded at 213 K, in conditions in which the chemical exchange is blocked but the scalar couplings persists practically unchanged, clearly confirms that the cross peaks present in the $^{31}P\{^1H\}$ EXSY spectrum recorded at 298 K are because of chemical exchanges.

(43) In fact, phenyl migration from P5 to P2 for complex **4** should result in the new species $[(PPh_3)(R_F)_2Pt(\mu\text{-}PPhEt)Pd(\mu\text{-}PPh_2)(\mu\text{-}Ph_2P\text{-}PPh_2)Pt(R_F)_2]$ which was never detected when a solution of **4**, kept at 298 K for 2 days, was cooled down to 213 K and analysed by $^{31}P\{^1H\}$ NMR.

Scheme 5

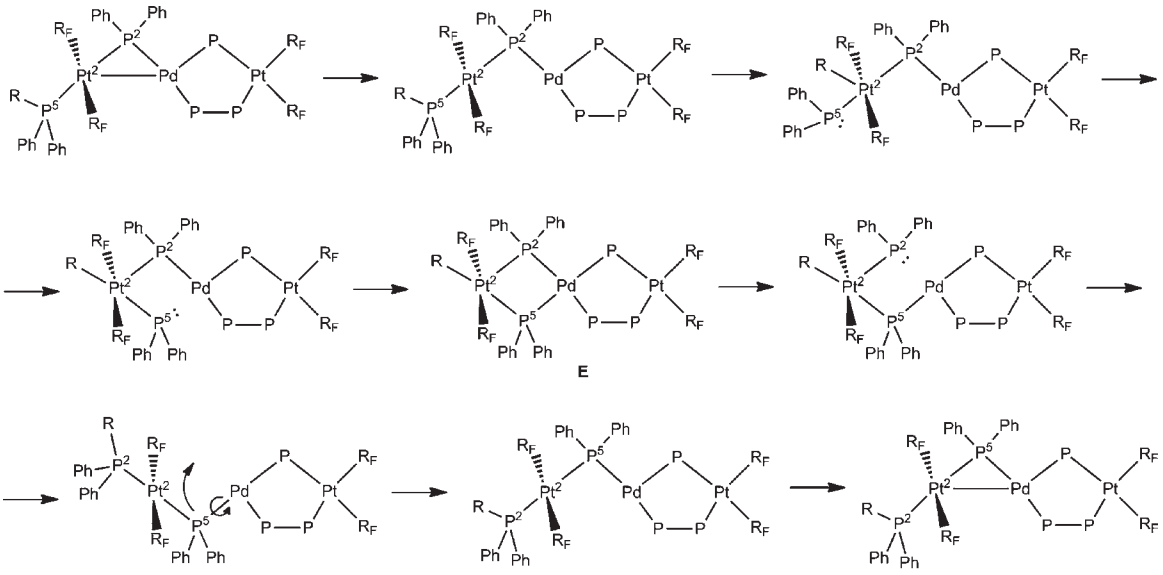

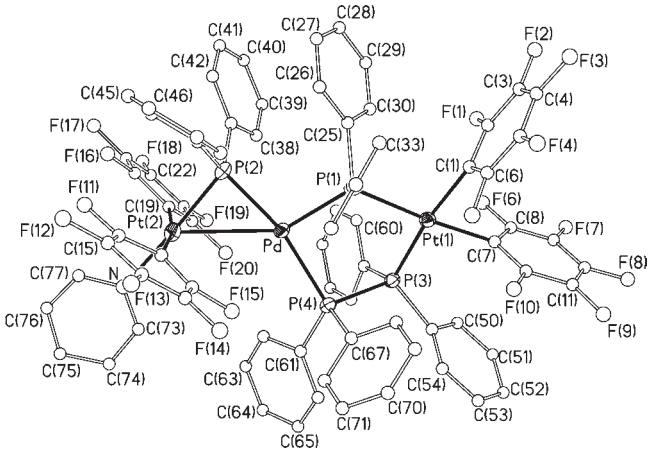

Figure 9. Molecular structure of the *trans* isomer of complex $[(py)(R_F)_2\text{-}Pt(\mu\text{-}PPh_2)Pd(\mu\text{-}PPh_2)(\mu\text{-}Ph_2P\text{-}PPh_2)Pt(R_F)_2]$ (**7**-*trans*).

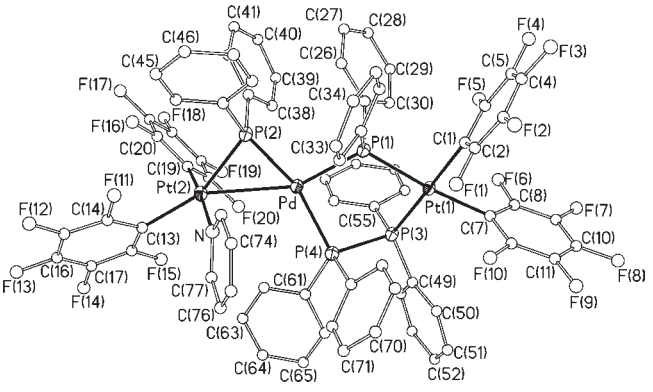

Figure 10. Molecular structure of the cis isomer of complex $[(py)(R_F)_2\text{-}Pt(\mu\text{-}PPh_2)Pd(\mu\text{-}PPh_2)(\mu\text{-}Ph_2P\text{-}PPh_2)Pt(R_F)_2]$ (**7**-*cis*).

crystals could be obtained by handmade selection, and a XRD analyses **7**-*cis* was also carried out.

The crystal structures of **7**-*trans* and **7**-*cis* are shown in Figures 9 and 10, respectively. Crystal data and other details of the structure analyses are reported in Table 1. Selected bond distances and angles are shown in Tables 5 and 6. In the two isomers the fragment "$Pd(\mu\text{-}P(1)Ph_2)(\mu\text{-}Ph_2P\text{-}PPh_2)Pt(1)(C_6F_5)_2$" is very similar and also similar to the analogous described for complexes **3** and **6**. The disposition of the Pt(2) and its environment with respect to the "$Pd(\mu\text{-}P(1)Ph_2)(\mu\text{-}Ph_2P\text{-}PPh_2)Pt(1)(C_6F_5)_2$" fragment is also similar. The main difference between the two isomers of **7** is the geometry of the ligands around Pt(2). While in **7**-*trans* the two pentafluorophenyl groups are mutually trans, in **7**-*cis*, they are disposed in a cis fashion.

However, the different geometry around Pt(2) does not cause important modification of the main structural parameters. Thus, in both cases the environment of Pt(2) is a conventional square plane and the Pt(2)−Pd distances are very similar (3.057(1) Å for **7**-*trans* and 2.977(1) Å for **7**-*cis*). These distances, indicative of the existence of an intermetallic bond, are intermediate between the ones for **3**, which contains a bulky PPh_3 ligand (cf., 3.237(1) Å), and **6**, which contains a small CO ligand (cf., 2.862(1) Å). This is again a proof of the flexibility of this kind of complexes that are able to adapt their geometry to the steric requirements of the ligands supported by Pt(2). In the case of the pyridine ligand present in the two isomers of complex **7**, its size seems to be in the verge in which the energetic difference between a trans or a cis disposition is not important and both species are formed and crystallized. With bulkier ligands, such as PPh_3 or PPh_2Et, the

Table 5. Selected Bond Distances (Å) and Angles (deg) for [(py)$(R_F)_2$Pt(μ-PPh_2)Pd(μ-PPh_2)(μ-Ph_2P-PPh_2)Pt$(R_F)_2$] (**7**-*trans*)

Pt(1)−C(7)	2.059(6)	Pt(1)−C(1)	2.074(5)	Pt(1)−P(3)	2.2813(13)
Pt(1)−P(1)	2.3541(14)	Pt(2)−C(19)	2.060(7)	Pt(2)−C(13)	2.083(6)
Pt(2)−N	2.133(5)	Pt(2)−P(2)	2.2654(15)	Pt(2)−Pd	3.0571(4)
Pd−P(2)	2.2711(15)	Pd−P(1)	2.3088(14)	Pd−P(4)	2.4157(14)
P(3)−P(4)	2.2289(19)				

C(7)−Pt(1)−C(1)	82.7(2)	C(7)−Pt(1)−P(3)	90.47(16)
C(1)−Pt(1)−P(3)	172.70(14)	C(7)−Pt(1)−P(1)	174.07(16)
C(1)−Pt(1)−P(1)	91.43(14)	P(3)−Pt(1)−P(1)	95.37(5)
C(19)−Pt(2)−C(13)	168.2(2)	C(19)−Pt(2)−N	86.8(2)
C(13)−Pt(2)−N	88.9(2)	C(19)−Pt(2)−P(2)	93.67(18)
C(13)−Pt(2)−P(2)	90.14(15)	P(2)−Pd−P(1)	102.89(5)
P(2)−Pd−P(4)	166.37(5)	P(1)−Pd−P(4)	90.68(5)

Table 6. Selected Bond Distances (Å) and Angles (deg) for [(py)$(R_F)_2$Pt(μ-PPh_2)Pd(μ-PPh_2)(μ-Ph_2P-PPh_2)Pt$(R_F)_2$]·1.4CH_2Cl_2 (**7**-*cis*·1.4CH_2Cl_2)

Pt(1)−C(7)	2.070(5)	Pt(1)−C(1)	2.073(5)	Pt(1)−P(3)	2.2791(14)
Pt(1)−P(1)	2.3477(14)	Pt(2)−C(19)	2.019(5)	Pt(2)−C(13)	2.091(5)
Pt(2)−N	2.129(5)	Pt(2)−P(2)	2.3194(15)	Pt(2)−Pd	2.9773(5)
Pd−P(2)	2.2241(14)	Pd−P(1)	2.3305(15)	Pd−P(4)	2.3556(15)
P(3)−P(4)	2.230(2)				

C(7)−Pt(1)−C(1)	83.8(2)	C(7)−Pt(1)−P(3)	96.52(15)
C(1)−Pt(1)−P(3)	177.73(16)	C(7)−Pt(1)−P(1)	173.03(15)
C(1)−Pt(1)−P(1)	89.23(14)	P(3)−Pt(1)−P(1)	90.41(5)
C(19)−Pt(2)−C(13)	86.0(2)	C(19)−Pt(2)−N	173.5(2)
C(13)−Pt(2)−N	89.0(2)	C(19)−Pt(2)−P(2)	88.46(16)
C(13)−Pt(2)−P(2)	157.21(16)	N−Pt(2)−P(2)	97.73(14)
P(2)−Pd−P(1)	105.26(5)	P(2)−Pd−P(4)	162.38(5)
P(1)−Pd−P(4)	92.15(5)		

sterical hindrance leads to a preferred trans pentafluorophenyl disposition, as observed in **3**, whereas the tiny CO allows a cis pentafluorophenyl arrangement and a shorter intermetallic distance.

The $^{31}P\{^1H\}$ NMR spectrum of **7**-*trans* at room temperature show four sharp signals (the P(2) signal appears at 106.5 ppm) and the same pattern is observed for the spectrum at 183 K. All data are given in Experimental Section. The spectrum of samples of **7**-*trans* with some amount of **7**-*cis* shows at room temperature a very broad signal centered at ~153 ppm due to P(2) atom of **7**-*cis*, and this signal is resolved in a doublet of doublets centered at 156 ppm at 183 K. Signals due to P(1), P(3), and P(4) of **7**-*cis* appear overlapped with those due to **7**-*trans*.

Addition of Acetonitrile to Complexes 4 and 6. Complexes **3**−**7** are unsaturated species with 46-valence electron count. In order to explore the possibility of reaching 48 VEC saturated complexes, we studied the reactivity of **3**, **4** and **6** toward several ligands. While bulky ligands such as PPh_2R (R = Ph, Et) did not add to **3** or **4**, small molecules such as acetonitrile smoothly reacted with **4** or **6**.

When two drops of acetonitrile were added to a red solution of **4** or **6** in $CDCl_3$ the color of the solution turned orange and the complexes [(L)$(R_F)_2$Pt(μ-PPh_2)Pd(MeCN)-(μ-PPh_2)(μ-Ph_2P-PPh_2)Pt$(R_F)_2$] (L = PPh_2Et **8**, CO **9**) were isolated as orange solids. Their crystal structures confirm the coordination of the acetonitrile to the Pd center in both cases. The structures of **8** and **9**, determined by X-ray diffraction methods, are shown in Figures 11 and 12, respectively. Crystal data and other details of the structure analyses are reported in Table 7. Selected bond distances and angles are shown in Tables 8 and 9. The structures of **8** and **9** are quite similar, with the acetonitrile ligand occupying the fourth coordination position of the Pd atom, which displays a conventional square planar environment. The total valence electron count for **8** and **9** is 48, and thus no Pt(2)−Pd bond is observed, (distances

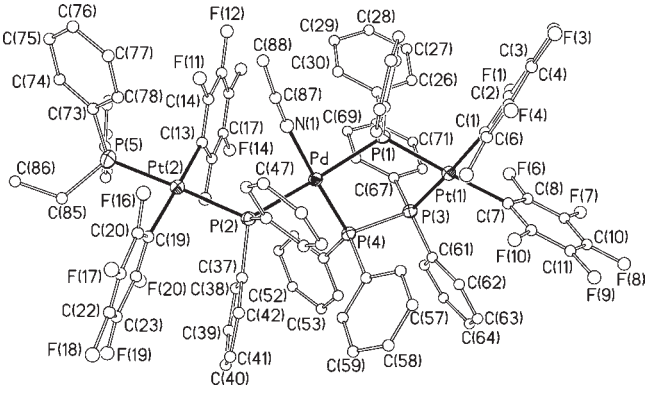

Figure 11. Molecular structure of complex [$(PEtPh_2)(R_F)_2$Pt(μ-PPh_2)-Pd(MeCN)(μ-PPh_2)(μ-Ph_2P-PPh_2)Pt$(R_F)_2$] (**8**).

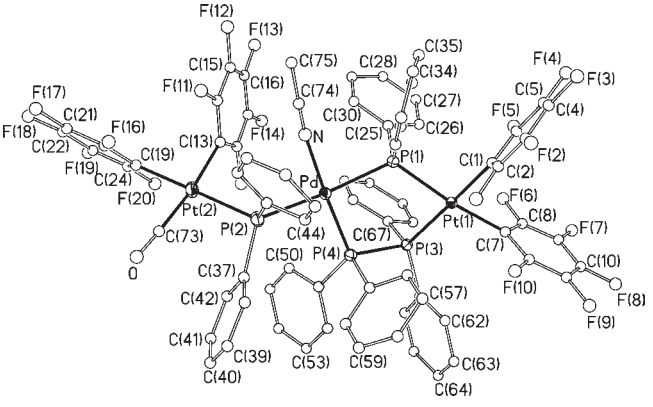

Figure 12. Molecular structure of complex [(CO)$(R_F)_2$Pt(μ-PPh_2)Pd-(MeCN)(μ-PPh_2)(μ-Ph_2P-PPh_2)Pt$(R_F)_2$] (**9**).

4.182(1) Å in **8** and 4.166(1) Å in **9**, to be compared to the corresponding distances in the precursors of 3.237(1) Å in **3** and of 2.862(1) in **6**). A significant difference of the

Table 7. Crystal Data and Structure Refinement for Complexes $[(PEtPh_2)(R_F)_2Pt(\mu\text{-}PPh_2)Pd(MeCN)(\mu\text{-}PPh_2)(\mu\text{-}Ph_2P\text{-}PPh_2)Pt(R_F)_2]\cdot NCMe\cdot CH_2Cl_2$ (**8**·NCMe·CH_2Cl_2) and $[(CO)(R_F)_2Pt(\mu\text{-}PPh_2)Pd(MeCN)(\mu\text{-}PPh_2)(\mu\text{-}Ph_2P\text{-}PPh_2)Pt(R_F)_2]\cdot 2.6n\text{-}C_6H_{14}$ (**9**·2.6*n*-C_6H_{14})

	8·NCMe·CH_2Cl_2	**9**·2.6*n*-C_6H_{14}
formula	$C_{88}H_{56}F_{20}NP_5PdPt_2NCMe\cdot CH_2Cl_2$	$C_{75}H_{43}F_{20}NOP_4PdPt_2\cdot 2.6n\text{-}C_6H_{14}$
M_t [g mol^{-1}]	2284.75	2198.61
T [K]	100(1)	100(1)
λ [Å]	0.71073	0.71073
crystal system	monoclinic	triclinic
space group	$C2/c$	P-1
a [Å]	42.303(6)	12.0400(4)
b [Å]	17.555(3)	15.5046(6)
c [Å]	23.354(3)	24.3942(6)
α [deg]	90	85.339(2)
β [deg]	92.671(3)	84.915(2)
γ [deg]	90	6.108(3)°
V [Å^3]	17324(4)	4394.7(2)
Z	8	2
ρ [g cm^{-3}]	1.752	1.661
μ [mm^{-1}]	3.672	3.539
F(000)	8896	2418
2θ range [deg]	2.5−50.1	7.5−50.2
no. of reflns collected	45 876	43 917
no. of unique reflns	15 274	15 556
R(int)	0.0468	0.0301
final R indices [$I > 2\sigma(I)$][a]		
R_1	0.0464	0.0307
R_2	0.1233	0.0790
R indices (all data)		
R_1	0.0675	0.0437
R_2	0.1363	0.0835
GOF on F^2[b]	1.049	1.029

[a] $R_1 = \sum(|F_o| - |F_c|)/\sum|F_o|$. $R_2 = [\sum w(F_o^2 - F_c^2)^2/\sum w(F_o^2)^2]^{1/2}$. [b] GOF $= [\sum w(F_o^2 - F_c^2)^2/(n_{obs} - n_{param})]^{1/2}$.

Table 8. Selected Bond Distances (Å) and Angles (deg) for $[(PEtPh_2)(R_F)_2Pt(\mu\text{-}PPh_2)Pd(MeCN)(\mu\text{-}PPh_2)(\mu\text{-}Ph_2P\text{-}PPh_2)Pt(R_F)_2]\cdot NCMe\cdot CH_2Cl_2$ (**8**·NCMe·CH_2Cl_2)

Pt(1)−C(1)	2.059(7)	Pt(1)−C(7)			
Pt(1)−P(1)	2.337(2)	Pt(2)−C(13)	2.056(8)	Pt(2)−C(19)	2.066(8)
Pt(2)−P(5)	2.288(2)	Pt(2)−P(2)	2.361(2)	Pd−N(1)	2.074(6)
Pd−P(4)	2.2528(19)	Pd−P(1)	2.419(2)	Pd−P(2)	2.430(2)
P(3)−P(4)	2.243(3)				
C(1)−Pt(1)−C(7)	85.3(3)	C(1)−Pt(1)−P(3)	175.5(2)		
C(7)−Pt(1)−P(3)	96.7(2)	C(1)−Pt(1)−P(1)	91.7(2)		
C(7)−Pt(1)−P(1)	176.9(2)	P(3)−Pt(1)−P(1)	86.34(7)		
C(13)−Pt(2)−C(19)	175.9(4)	C(13)−Pt(2)−P(5)	87.9(2)		
C(19)−Pt(2)−P(5)	90.0(2)	C(13)−Pt(2)−P(2)	93.5(2)		
C(19)−Pt(2)−P(2)	88.6(2)	P(5)−Pt(2)−P(2)	178.34(7)		
N(1)−Pd−P(4)	177.02(18)	N(1)−Pd−P(1)	86.38(17)		
P(4)−Pd−P(1)	90.77(7)	N(1)−Pd−P(2)	82.82(17)		
P(4)−Pd−P(2)	99.71(7)	P(1)−Pd−P(2)	161.90(7)		

Table 9. Selected Bond Distances (Å) and Angles (deg) for $[(CO)(R_F)_2Pt(\mu\text{-}PPh_2)Pd(MeCN)(\mu\text{-}PPh_2)(\mu\text{-}Ph_2P\text{-}PPh_2)Pt(R_F)_2]\cdot 2.6n\text{-}C_6H_{14}$ (**9**·2.6*n*-C_6H_{14})

Pt(1)−C(7)	2.058(5)	Pt(1)−C(1)	2.060(5)	Pt(1)−P(3)	2.2634(12)
Pt(1)−P(1)	2.3315(12)	Pt(2)−C(73)	1.878(7)	Pt(2)−C(13)	2.048(5)
Pt(2)−C(19)	2.070(6)	Pt(2)−P(2)	2.3622(14)	Pd−N	2.073(4)
Pd−P(4)	2.2389(13)	Pd−P(1)	2.4044(13)	Pd−P(2)	2.4201(13)
C(7)−Pt(1)−C(1)	85.14(18)	C(7)−Pt(1)−P(3)	97.03(13)		
C(1)−Pt(1)−P(3)	176.84(14)	C(7)−Pt(1)−P(1)	172.54(13)		
C(1)−Pt(1)−P(1)	91.50(13)	P(3)−Pt(1)−P(1)	86.60(4)		
C(73)−Pt(2)−C(13)	173.4(2)	C(73)−Pt(2)−C(19)	89.1(2)		
C(13)−Pt(2)−C(19)	84.9(2)	C(73)−Pt(2)−P(2)	90.64(18)		
C(13)−Pt(2)−P(2)	95.40(15)	C(19)−Pt(2)−P(2)	179.51(17)		
N−Pd−P(4)	175.23(12)	N−Pd−P(1)	87.42(12)		
P(4)−Pd−P(1)	89.89(4)	N−Pd−P(2)	83.62(12)		
P(4)−Pd−P(2)	98.24(5)	P(1)−Pd−P(2)	165.89(5)		

structures of **8** and **9** with respect to their precursors is the disposition of the phosphanido ligand singly bridging the Pd and Pt(2). Thus, while in the precursors **3** and **6** this PPh_2 group is trans to the diphosphane bridging ligand, in **8** and **9**, it is trans to the other diphenylphosphanido group.

The $^{31}P\{^1H\}$ NMR spectra show that the P(2) signal appearing at δ 121 (**4**) and δ 151 (**6**) in the starting complexes, shift toward higher fields, at δ 5.1 and δ −10.1 respectively, indicating that, as previously commented, there is not a metal−metal bond.[14,44−46]

The easy elimination of the acetonitrile ligand in transition-metal complexes is a commonly observed process,[47,48] and complexes **8** and **9** lose the CH_3CN ligand both in solution and in the solid state. Thus, the $^{31}P\{^1H\}$

spectrum obtained dissolving crystals of **8** in $CDCl_3$ showed the signals of both **8** and its precursor **4** in equilibrium (^{31}P EXSY) while in the IR spectrum of solid samples of **9**, the absorptions assignable to the $\nu(C\equiv O)$ vibration of complex **6** is also observed. Therefore, in the solutions of **9** prepared for NMR assignments or for crystal growing, a drop of acetonitrile was always added. The coordination/decoordination of acetonitrile in complex **6**/**9** confirms that the saturation of the Pd center in these complexes can be carried out either by formation of Pd−N or Pd−Pt(2) bonds. The square coordination planes of Pd and Pt(2) in **9** form an angle of 62.6(1)° and the Pt(2)−Pd separation is 4.182(1) Å, which is longer than the analogous one found in **3** (3.237(1) Å). A significant difference is the disposition of the P(2) phosphanido ligand, which is located trans the P(1) group to favor the placement of the acetonitrile around the Pd center in this very crowded complex.

Concluding Remarks

The study proves that $AgClO_4$ and $[AgOClO_3(PPh_3)]$ act always as oxidants toward $[NBu_4]_2[(R_F)_2Pt(\mu\text{-}PPh_2)_2M(\mu\text{-}PPh_2)_2Pt(R_F)_2]$ (M = Pt, Pd. $R_F = C_6F_5$) and in no case are adducts between the $[(R_F)_2Pt(\mu\text{-}PPh_2)_2M(\mu\text{-}PPh_2)_2Pt(R_F)_2]^{2-}$ and $Ag(PPh_3)^+$ fragment observed. Steric effects are held responsible for (i) the different geometries exhibited by the ligands around Pt^2 in **3**−**4** with respect to **5**−**6** to allow the bulkiest ligand to stay trans to μ-P^2, (ii) the observed formation of both cis- and trans-isomers of the pyridine complex **7**, (iii) the complex dynamic behavior exhibited by complexes **3** and **4**, and (iv) the precluded incorporation of an additional phosphane (but not of CH_3CN) in complexes **3** and **4**.

A "through space" $^{19}F-^{31}P$ spin−spin coupling between the neighboring F(20) and P(4) in complexes **3** and **4** is held responsible for the $^{TS}J_{P,F}$ of ca. 55 Hz observed at low temperature.

Experimental Section

General Comments. C, H, and N analyses were performed with a Perkin-Elmer 240B microanalyzer. IR spectra were recorded on a Perkin-Elmer Spectrum One spectrophotometer (Nujol mulls between polyethylene plates in the range 4000−350 cm^{-1}). NMR spectra in solution were recorded on a Varian Unity 300 or Bruker Avance 400 spectrometers with $SiMe_4$, $CFCl_3$ and 85% H_3PO_4 as external references for ^1H, ^{19}F and ^{31}P, respectively. Literature methods were used to prepare the starting materials $[PdPt_2(\mu\text{-}PPh_2)_2(\mu\text{-}Ph_2P\text{-}PPh_2)(R_F)_4]$,[13] $[NBu_4]_2[(R_F)_2Pt(\mu\text{-}PPh_2)_2M(\mu\text{-}PPh_2)_2Pt(R_F)_2]$ (M = Pt, Pd),[11] and $[AgOClO_3(PPh_3)]$.[49]

Safety Note. Perchlorate salts of metal complexes with organic ligands are potentially explosive. Only small amounts of materials should be prepared and these should be handled with great caution.

Reaction of $[NBu_4]_2[(R_F)_2Pt(\mu\text{-}PPh_2)_2Pt(\mu\text{-}PPh_2)_2Pt(R_F)_2]$ with $[Ag(OClO_3)PPh_3]$. To a yellow solution of $[NBu_4]_2[(R_F)_2Pt(\mu\text{-}PPh_2)_2Pt(\mu\text{-}PPh_2)_2Pt(R_F)_2]$ (**1b**) (0.200 g, 0.080 mmol) in acetone (20 mL) was added $[Ag(OClO_3)PPh_3]$ (0.076 g, 0.160 mmol), and the mixture was stirred for 2 h at room temperature. This produces a red solution and a silver mirror. After filtration, the solution was evaporated to 1 mL. $CHCl_3$ (10 mL) was added and evaporated to ~8 mL. After 8 h in the freezer the red solid was filtered off and washed with $CHCl_3$. $[(R_F)_2Pt^{III}(\mu\text{-}PPh_2)_2Pt^{III}(\mu\text{-}PPh_2)_2Pt(R_F)_2]$,[11] 0,138 g, 83% yield.

Synthesis of 3. A. By Reaction of 1a with $[Ag(OClO_3)PPh_3]$. To an orange suspension of **1a** (0.250 g, 0.104 mmol) in 30 mL of CH_2Cl_2 (or an orange solution in 15 mL of acetone) was added $[Ag(OClO_3)PPh_3]$ (0.098 g, 0.209 mmol) and the mixture was stirred at room temperature for 2 h giving rise to a red solution along with a silver mirror. The mixture was filtered off and the solution evaporated to approximately 2 mL. ^{i}PrOH (2 mL) was added and the red solid was filtered off and washed with 2 × 1 mL of cold acetone. **3**, 0.115 g, 51% yield. Found: C, 49.86; H, 2.63. $C_{90}F_{20}H_{55}P_5PdPt_2$ requires C, 49.82; H, 2.54 $^{31}P\{^1H\}$ NMR (121.4 MHz, CD_2Cl_2, 193 K, H_3PO_4): δ = 120.6 (ddd, P2, $^1J_{(Pt2,P2)}$ = 1680 Hz), 70.9 (ddd, P4, $^2J_{(Pt1,P4)}$ = 292 Hz), 47.1 (d, P1, $^1J_{(Pt1,P1)}$ = 2038 Hz), 45.0 (d, P3, $^1J_{(Pt1,P3)}$ = 2487 Hz), 17.7 (d, P5, $^1J_{(Pt2,P5)}$ = 2525 Hz) ppm. $^2J_{(P1,P2)}$ = 48, $^2J_{(P2,P4)}$ = 270, $^2J_{(P2,P5)}$ = 290, $^1J_{(P3,P4)}$ = 183, $J_{(o\text{-}F20,P4)}$ = 55 Hz). ^{19}F NMR (282.4 MHz, CD_2Cl_2, 193 K, $CFCl_3$): δ = -98.0 ($J_{(Pt,F)}$ = 351 Hz, 1*o*-F), −108.9 (1*o*-F), −114.9 ($J_{(Pt,F)}$ = 347 Hz, 1*o*-F), −115.5 (2*o*-F), −115.9 (1*o*-F), −116.8 ($J_{(Pt-F)}$ = 304 Hz, 2*o*-F), −160.5 (1F), −161.0 (1F), −162.3 (1F), −162.7 (3F), −163.2 (1F), −163.3 (1F), −163.8 (1F), −164.3 (1F), −164.5 (1F), −164.9 (1F) ppm.

B. By Reaction of 2 with PPh_3. To a suspension of **2** (0.120 g, 0.063 mmol) in CH_2Cl_2 (15 mL) PPh_3 was added (0.017 g, 0.063 mmol), and the mixture was stirred for 15 h at room temperature. The red solution was evaporated to ~2 mL, while **3** crystallized as a red solid. 0.104 g, 76% yield.

C. By Reaction of 1a with $AgClO_4$ and PPh_3. To an acetone (30 mL) solution of **1a** (0.120 g, 0.050 mmol) was added PPh_3 (0.014 g, 0.053 mmol) and $AgClO_4$ (0.022 g, 0.106 mmol). After 2 h stirring at room temperature the mixture was filtered and the solution evaporated to approximately 2 mL. ^{i}PrOH (3 mL) was added and the red solid was filtered off and washed with 3 × 1 mL of ^{i}PrOH. **3**, 0.045 g, 42% yield.

Synthesis of 4. A. By Reaction of 1a with $AgClO_4$ and PPh_2Et. To an acetone (30 mL) solution of **1a** (0.150 g, 0.063 mmol) was added PPh_2Et (0.016 μL, 0.077 mmol), and $AgClO_4$ (0.027 g, 0.130 mmol). After it was stirred for 2 h at room temperature, the mixture was filtered and the solution evaporated to approximately 2 mL. ^{i}PrOH (3 mL) was added and the red solid was filtered off and washed with 3 × 1 mL of ^{i}PrOH. **4**, 0.035 g, 26% yield. Found: C, 48.60; H, 2.49. $C_{86}F_{20}H_{55}P_5PdPt_2$ requires C, 48.68; H, 2.59. $^{31}P\{^1H\}$ NMR (121.4 MHz, $CDCl_3$, 213 K, H_3PO_4): δ = 121.0 (ddd, P2 $^1J_{(Pt2,P2)}$ = 1577 Hz), 67.0 (ddd, P4, $^2J_{(Pt1,P4)}$ = 254 Hz), 45.0 (d, P1, $^1J_{(Pt1,P1)}$ = 1882 Hz), 41.5 (d, P3, $^1J_{(Pt1,P3)}$ = 2431 Hz), 15.8 (d, P5, $^1J_{(Pt2,P5)}$ = 2513 Hz) ppm. $^2J_{(P1,P2)}$ = 46, $^2J_{(P2,P4)}$ = 275, $^2J_{(P2,P5)}$ = 285, $^1J_{(P3,P4)}$ = 178, $J_{(o\text{-}F20,P4)}$ = 55 Hz). ^{19}F NMR (282.4 MHz, $CDCl_3$, 213 K, $CFCl_3$, *o*- *m*- and *p*-F atoms of each A-D ring assigned by a ^{19}F -^{19}F COSY and EXSY experiments): δ = −99.4 ($J_{(Pt,F)}$ = 375 Hz, 1 *o*-F20, D), −111.0 (1 *o*-F15, C), −114.4 (1 *o*-F11, C), −115.4 (1 *o*-F16, D + 1 *o*-F, A), −115.7 (1 *o*-F, B), −116.2 (1 *o*-F, B), −116.5 ($J_{(Pt,F)}$ = 293 Hz, 1 *o*-F, A), −161.1 (1 *p*-F, D + 1 *m*-F, D), −161.6 (1 *p*-F, C), −161.8 (1 *p*-F, B), −162.1 (1 *p*-F,A), −162.3 (1 *m*-F, C), −162.6 (1 *m*-F, D), −162.9 (1 *m*-F, A), −163.3 (1 *m*-F, C), −163.7 (1 *m*-F, A), −163.8 (1 *m*-F, B), −164.4 (1 *m*-F, B) ppm.

B. By Reaction of 2 with PPh_2Et. To a suspension of **2** (0.120 g, 0.063 mmol) in CH_2Cl_2 (15 mL) $PEtPh_2$ was added (13 μL, 0.063 mmol) and the mixture was stirred for 16 h at room temperature. The red solution was evaporated to ~1 mL, and

(44) Alonso, E.; Forniés, J.; Fortuño, C.; Martín, A.; Rosair, G. M.; Welch, A. J. *Inorg. Chem.* **1997**, *36*, 4426–4431.
(45) Alonso, E.; Forniés, J.; Fortuño, C.; Martín, A.; Orpen, A. G. *Organometallics* **2003**, *22*, 2723–2728.
(46) Ara, I.; Chaouche, N.; Forniés, J.; Fortuño, C.; Kribii, A.; Tsipis, A. C. *Organometallics* **2006**, *25*, 1084–1091.
(47) Murahashi, T.; Nagai, T.; Okuno, T.; Matsutani, T.; Kurosawa, H. *Chem. Commun.* **2000**, 1689–1690.
(48) Ara, I.; Chaouche, N.; Forniés, J.; Fortuño, C.; Kribii, A.; Martín, A. *Eur. J. Inorg. Chem.* **2005**, 3894–3901.
(49) Cotton, F. A.; Falvello, L. R.; Usón, R.; Forniés, J.; Tomás, M.; Casas, J. M.; Ara, I. *Inorg. Chem.* **1987**, *26*, 1366–1370.

hexane (3 mL) was added. A red crystallized solid, which was filtered and washed with hexane (3 × 0.5 mL), **4**, 0.126 g, 95% yield.

Synthesis of 6. A red suspension of **2** (0.150 g, 0.079 mmol) in CH_2Cl_2 was stirred at room temperature under a CO atmosphere for 9 h. The red solution was evaporated to ca. 1 mL and hexane (3 mL) was added. A red solid, **6**, crystallized and was filtered and washed with hexane (3 × 0.5 mL), 0.085 g, 56% yield. Found: C, 45.31; H, 2.07. $C_{73}F_{20}H_{40}OP_4PdPt_2$ requires C, 45.34; H, 2.09. IR, solid state 2087 cm^{-1}; CH_2Cl_2 solution 2095 and 2083 cm^{-1} ν(C≡O). $^{31}P\{^1H\}$ NMR (121.4 MHz, CD_2Cl_2, 183 K, H_3PO_4): δ = 150.5 (dd, P2, $^1J_{(Pt2,P2)}$ = 1224 Hz), 58.9 (dd, P4, $^2J_{(Pt1,P4)}$ = 234 Hz), 49.4 (d, P3, $^1J_{(Pt1,P3)}$ = 2358 Hz), 42.5 (d, P1, $^1J_{(Pt1,P1)}$ = 1975 Hz) ppm. $^2J_{(P1,P2)}$ = 46 Hz, $^2J_{(P2,P4)}$ = 281 Hz, $^1J_{(P3,P4)}$ = 165 Hz.).

Synthesis of 7. A red suspension of **2** (0.120 g, 0.063 mmol) in CH_2Cl_2 and pyridine (20 μL, 0.248 mmol) was stirred at room temperature for 22 h. The red solution was evaporated to ca. 1 mL and hexane (3 mL) was added. A red solid, **7**-*trans*, crystallized and was filtered and washed with hexane (3 × 0.5 mL), 0.073 g, 58% yield. Found: C, 46.41; H, 2.20; N, 0.83. $C_{77}F_{20}H_{45}NP_4PdPt_2$ requires C, 46.60; H, 2.28; N, 0.71. $^{31}P\{^1H\}$ NMR (121.4 MHz, CD_2Cl_2, 183 K, H_3PO_4): δ = 114.1 (dd, P2, $^1J_{(Pt2,P2)}$ = 2460 Hz), 64.9 (dd, P4, $^2J_{(Pt1,P4)}$ = 304 Hz), 50.7 (d, P3, $^1J_{(Pt1,P3)}$ = 2438 Hz), 29.6 (d, P1, $^1J_{(Pt1,P1)}$ = 1948 Hz) ppm. $^2J_{(P1,P2)}$ = 52 Hz, $^2J_{(P2,P4)}$ = 296 Hz, $^1J_{(P3,P4)}$ = 178 Hz.). $^{31}P\{^1H\}$ NMR (121.4 MHz, CD_2Cl_2, 293 K, H_3PO_4): δ = 106.5 (dd, P2, $^1J_{(Pt2,P2)}$ = 2449 Hz), 66.9 (dd, P4, $^2J_{(Pt1,P4)}$ = 277 Hz), 47.7 (d, P3, $^1J_{(Pt1,P3)}$ = 2424 Hz), 37.4 (d, P1, $^1J_{(Pt1,P1)}$ = 1962, $^2J_{(Pt2,P1)}$ = 282 Hz) ppm. $^2J_{(P1,P2)}$ = 50 Hz, $^2J_{(P2,P4)}$ = 299 Hz, $^1J_{(P3,P4)}$ = 180 Hz. ^{19}F NMR (282.4 MHz, CD_2Cl_2, 183 K, $CFCl_3$): δ = −106.8 (1*o*-F), −108.1 (1*o*-F), −115.1 ($J_{(Pt,F)}$ = 308 Hz, 1*o*-F), −116.2 ($J_{(Pt,F)}$ = 230 Hz, 1*o*-F), −116.9 (1*o*-F), −118.1 (1*o*-F), −118.6 (1*o*-F), −118.8 ($J_{(Pt,F)}$ = 158 Hz, 1*o*-F), −158.3 (1 *p*-F), −158.9 (1 *m*-F), −161.2 (1 *m*-F), −161.5 (1 *p*-F), −162.7 (1 *p*-F), −163.3 (4F), −163.9 (1 *m*-F), −164.2 (1 *m*-F), −164.9 (1 *m*-F) ppm. ^{19}F NMR (282.4 MHz, CD_2Cl_2, 293 K, $CFCl_3$): δ = −113.6 (2*o*-F), −116.3 ($J_{(Pt,F)}$ = 299 Hz, 3*o*-F), −116.7 ($J_{(Pt,F)}$ = 293 Hz, 3*o*-F), −160.5 (2F), −162.4 (4F), −163.3 (*1p*-F), −163.5 (1 *p*-F), −164.5 (2F), −165.0 (2F), ppm. The red filtrate was left in the freezer for a week. A red solid was filtered and washed with 0.5 mL of hexane, 0.018 g, mixture of **7**-*trans* (main component) and **7**-*cis*. **7**-*cis*: $^{31}P\{^1H\}$ NMR (121.4 MHz, CD_2Cl_2, 183 K, H_3PO_4): δ = 155.6 (dd, P2, $^1J_{(Pt2,P2)}$ = 1618 Hz), 33.4 (d, P1, $^1J_{(Pt1,P1)}$ = 1918 Hz) ppm. $^2J_{(P1,P2)}$ = 47 Hz, $^2J_{(P2,P4)}$ = 280 Hz. The P4 and P3 signals appear overlapped with those due to complex **7**-*trans* and data can not be unambiguously extracted.

Synthesis of 8. To a red solution of **4** (0.073 g, 0.034 mmol) in $CHCl_3$ (5 mL) 1 mL of MeCN was added and the color of the solution became orange. After 30 min stirring, at room temperature, the solution was evaporated to ∼1 mL and left in the freezer for 10 h. An orange solid crystallized and was filtered off and dried. **8**, 0.049 g, 66% yield. Found: C, 48.78; H, 2.40; N, 066. $C_{88}F_{20}H_{58}NP_5PdPt_2$ requires: C, 48.87; H, 2.68; N, 0.65. IR, solid state 2321 cm^{-1} ν(C≡N). $^{31}P\{^1H\}$ NMR (161.9 MHz, $CDCl_3$, 293 K, H_3PO_4): δ = 84.1 (d, P4, $^2J_{(Pt1,P4)}$ = 198 Hz), 80.7 (d, P3, $^1J_{(Pt1,P3)}$ = 2391 Hz), 29.3 (d, P1, $^1J_{(Pt1,P1)}$ = 1843 Hz), 9.6 (d, P5, $^1J_{(Pt2,P5)}$ = 2584 Hz), 5.1 (dd, P2, $^1J_{(Pt2,P2)}$ = 2043 Hz) ppm. $^2J_{(P1,P2)}$ = 222, $^2J_{(P2,P5)}$ = 351, $^1J_{(P3,P4)}$ = 119 Hz.

Synthesis of 9. To a red solution of **6** (0.037 g, 0.019 mmol) in CH_2Cl_2 (5 mL), 1 mL of MeCN was added causing a turning of the solution into yellow. After 30 min of stirring at room temperature, the solution was evaporated to ∼1 mL and **9** crystallized as a yellow solid, which was filtered and washed with cold acetonitrile (2 × 0.5 mL), 0.027 g, 72% yield. The partial loosing of acetonitrile precluded the elemental analysis. IR, solid state 2108 cm^{-1} ν(C≡O); 2322 cm^{-1} ν(C≡N). $^{31}P\{^1H\}$ NMR (161.9 MHz, $CDCl_3$, 293 K): δ = 89.4 (d, P4, $^2J_{(Pt1,P4)}$ = 323 Hz), 82.8 (d, P3, $^1J_{(Pt1,P3)}$ = 2414 Hz), 31.8 (d, P1, $^1J_{(Pt1,P1)}$ = 1850 Hz), −10.1 (d, P2, $^1J_{(Pt2,P2)}$ = 1581 Hz) ppm. $^2J_{(P1,P2)}$ = 245, $^1J_{(P3,P4)}$ = 130 Hz.

X-ray Structure Determinations. Crystal data and other details of the structure analysis are presented in Tables 1 and 7. Suitable crystals of **3**·CH_2Cl_2, **6**·0.75*n*-C_6H_{14}·0.2CH_2Cl_2, **7**-*trans*, **8**·NCMe·CH_2Cl_2 and **9**·2.6*n*-C_6H_{14} were obtained by slow diffusion of *n*-hexane into a CH_2Cl_2 solution of the complexes at 4 °C. Finally, slow diffusion at 4 °C of n-hexane into a CH_2Cl_2 solution of a mixture of **7**-*trans* and **7**-*cis* (Experimental) produces two types of crystals of different aspect, some dark red (**7**-*trans*) and other ones red. The selection of the less colored ones, allowed to study the X-ray structure of **7**-*cis*. Crystals were mounted at the end of a glass fiber. The diffraction data were collected in a Bruker Smart Apex CCD diffractometer for **3**·CH_2Cl_2, **6**·0.75*n*-C_6H_{14}·0.2CH_2Cl_2 and **7**·NCMe·CH_2Cl_2, and in an Oxford Diffraction Xcalibur CCD diffractometer for **7**-*trans*, **7**-*cis*·1.4CH_2Cl_2 and **9**·2.6*n*-C_6H_{14}. Unit cell dimensions were determined from the positions of 5166, 1010, 23876, 24010, 949, and 28665 reflections from the main data set respectively. For **3**·CH_2Cl_2, **6**·0.75*n*-C_6H_{14}·0.2CH_2Cl_2 and **8**·NCMe·CH_2Cl_2, the diffraction frames were integrated using the SAINT package[50] and corrected for absorption with SADABS.[51] For **7**-*trans*, **7**-*cis*·1.4CH_2Cl_2, and **9**·2.6*n*-C_6H_{14}, the diffraction frames were integrated and corrected for absorption using the Crysalis RED package.[52] Lorentz and polarization corrections were applied in all cases.

The structures were solved by Patterson and Fourier methods. All refinements were carried out using the SHELXL-97 program.[53] All non-hydrogen atoms were assigned anisotropic displacement parameters and refined without positional constraints except as noted below. All hydrogen atoms were constrained to idealized geometries and assigned isotropic displacement parameters 1.2 times the U_{iso} value of their attached carbon atoms (1.5 times for methyl hydrogen atoms). For **3**·CH_2Cl_2, the C−Cl distances of the dichlorometane solvent molecule were constrained to 1.74 Å, and the chlorine atoms were refined with a common set of thermal anisotropic parameters. For **6**·0.75*n*-C_6H_{14}·0.2CH_2Cl_2, very diffuse solvents were detected in the density maps and modeled as an *n*-hexane molecule (refined with 0.75 occupancy), and a CH_2Cl_2 molecule (refined with 0.20 occupancy). The interatomic distances in the solvent molecules were constrained to sensible values. A common set of anisotropic thermal parameters was used for the six C atoms of the *n*-hexane molecule. The C and Cl atoms of the CH_2Cl_2 molecule were refined isotropically, with the same thermal parameter for the two chlorine atoms. For **7**-*trans* the pyridine ring is disordered over two positions which are related by a rotation axis containing the N and C *para* atoms. The ortho and meta carbon and hydrogen atoms of the two component of the disorder were refined with 0.5 partial occupancy. For **7**-*cis*·1.4CH_2Cl_2, two molecules of dichloromethane were located from the density maps. One of these molecules needed constrains in their C−Cl distances and a common set of thermal anisotropic parameters were used for all the atoms of the moiety, which were refined with occupancy 0.4. For **8**·NCMe·CH_2Cl_2, geometric constraints were applied for the geometry of the two CH_2Cl_2 solvent molecules, which were refined with 0.5 occupancy. For **9**·2.6*n*-C_6H_{14}, several molecules of *n*-hexane were located from the density maps, some of which were near to inversion centers. Some of these molecules needed constraints in their geometrical parameters and, furthermore, in some cases

(50) *SAINT*, version 5.0; Bruker Analytical X-raySystems; Madison, WI, 2000.

(51) Sheldrick, G. M. *SADABS Empirical Absorption Program*; University of Göttingen: Göttingen, Germany, 1996.

(52) *CrysAlis RED. A program for Xcalibur CCD System X-ray Diffraction Data Reduction*; Oxford Diffraction Ltd.: Oxford, U.K., 2005.

(53) Sheldrick, G. M. *SHELXL-97, A Program for Crystal Structure Determination*; University of Göttingen: Göttingen, Germany, 1997.

common sets of thermal anisotropic parameters were used for all the C atoms of the moiety. Full-matrix least-squares refinement of these models against F^2 converged to the final residual indices given in Tables 1 and 7.

Acknowledgment. This work was supported by the Spanish MICINN (DGI)/FEDER (Project CTQ2008-06669-C02-01/BQU and the Gobierno de Aragón (Grupo de Excelencia: Química Inorgánica y de los Compuestos Organometálicos). S. I. gratefully acknowledges the grant provided by the Ministerio de Educación y Ciencia. Italian MIUR (PRIN project n. 2007 × 2RLL2) and COST PhoSciNet (project CM082) are also gratefully acknowledged.

Supporting Information Available: Further details of the structure determinations of **3**·CH_2Cl_2, **6**·0.75*n*-C_6H_{14}·0.2CH_2Cl_2, **7**-*trans*, **7**-*cis*, **8**·NCMe·CH_2Cl_2, and **9**·2.6*n*-C_6H_{14}, including atomic coordinates, bond distances and angles, and thermal parameters (CIF). This material is available free of charge via the Internet at http://pubs.acs.org